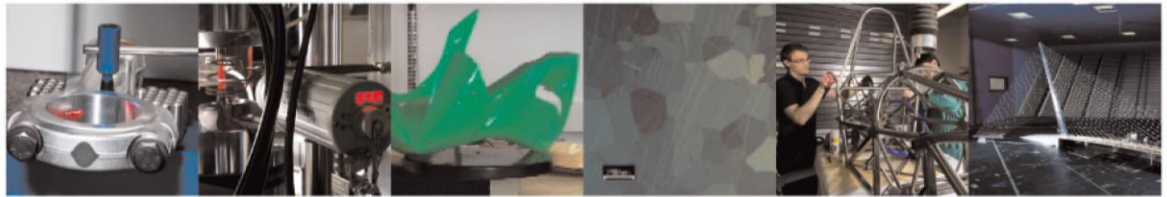




POLITECNICO
MILANO 1863

DIPARTIMENTO DI MECCANICA



Additive manufacturing and post-processing of superelastic NiTi micro struts as building blocks for cardiovascular stents

Finazzi, Valentina; Berti, Francesca; Petrini, Lorenza; Previtali, Barbara; Demir, Ali Gökhan

This is a post-peer-review, pre-copyedit version of an article published in Additive Manufacturing. The final authenticated version is available online at:

<http://dx.doi.org/10.1016/j.addma.2023.103561>

This content is provided under [CC BY-NC-ND 4.0](https://creativecommons.org/licenses/by-nc-nd/4.0/) license



Additive manufacturing and post-processing of superelastic NiTi micro struts as building blocks for cardiovascular stents

Valentina Finazzi (1,2), valentina.finazzi@polimi.it

Francesca Berti(3), francesca.berti@polimi.it

Lorenza Petrini (2), lorenza.petrini@polimi.it

Barbara Previtali (1), barbara.previtali@polimi.it

Ali Gökhan Demir* (1), aligokhan.demir@polimi.it

1. Department of Mechanical Engineering, Politecnico di Milano, Milan, Italy

2. Department of Civil and Environmental Engineering, Politecnico di Milano, Milan, Italy

3. Department of Chemistry, Materials and Chemical Engineering, Politecnico di Milano, Milan, Italy

*Corresponding author

Additive manufacturing and post-processing of superelastic NiTi micro struts as building blocks for cardiovascular stents

Valentina Finazzi (1,2), valentina.finazzi@polimi.it

Francesca Berti (3), francesca.berti@polimi.it

Lorenza Petrini (2), lorenza.petrini@polimi.it

Barbara Previtali (1), barbara.previtali@polimi.it

Ali Gökhan Demir (1)*, aligokhan.demir@polimi.it

1. Department of Mechanical Engineering, Politecnico di Milano, Milan, Italy

2. Department of Civil and Environmental Engineering, Politecnico di Milano, Milan, Italy

3. Department of Chemistry, Materials and Chemical Engineering, Politecnico di Milano, Milan, Italy

*Corresponding author

Abstract

Laser powder bed fusion (PBF-LB) can be potentially used for producing patient-specific biomedical devices based on micro struts such as cardiovascular stents. NiTi alloys are an appealing choice for their superelastic behaviour, while their processing with PBF-LB poses several challenges. The final component is expected to have the correct transition temperature and mechanical properties along with an acceptable surface finish. All of these properties require a complete manufacturing cycle from PBF-LB for the production of the geometrical form, to the heat treatment for the adjustment of the mechanical properties, and finally to the chemical etching for the reduction of surface roughness. Therefore this work studies a complete manufacturing cycle composed of PBF-LB process parameters, heat treatment recipes, and chemical etching conditions for producing NiTi micro struts with superelastic behaviour. Transition temperature measurements and tensile tests were applied to verify the influence of each manufacturing process on the material properties using ad-hoc designed micro strut geometries. The results showed previously unreported tensile superelasticity with micro struts at the end of the manufacturing cycle, once the PBF-LB process parameters were correctly selected, followed by heat treatment and chemical etching stages. The determined additive manufacturing chain was then used to produce demonstrator stent mesh with variable diameter and 130 μm strut thickness.

Keywords: Laser powder bed fusion; heat treatment; chemical etching; stent; micro additive manufacturing

1. Introduction

Additive manufacturing (AM) of patient-specific devices is a clinical reality for several applications such as cranial or orthopedic implants [1]. Laser powder bed fusion (PBF-LB) is a key additive manufacturing process commonly used for producing biomedical metal implants. Concerning additive manufacturing of metal implants, biomedical device manufacturing has arguably led to the development of the laser powder bed fusion (PBF-LB) process for implant materials such as AISI 316L [2], CoCr[3], and Ti6Al4V [4,5]. As the need for improved performance for a minimally invasive treatment is increased [6], the process capabilities of PBF-LB are pushed forward for novel materials and geometries. Strut-based biomedical devices such as cardiovascular stents can also benefit from the use of PBF-LB technology for producing innovative patient-specific implants.

A cardiovascular stent is conventionally produced by laser micro-cutting of tubular precursors [7]. Depending on the material type, braiding of thin wires is also a possibility [8]. These devices are characterized by small diameters (1-5 mm) and thin strut widths (0.05-0.3 mm). From the geometrical perspective, they pose several challenges for the PBF-LB process as the dimensions are similar to the powder size (15-50 μm) and the laser beam diameter (50-100 μm). Recent works showed that the PBF-LB process can be manipulated to produce stent-like geometries using CoCr [9], AISI 316L [10][11], Zn [12], and Fe [13]. The literature shows that with an adequate design for the AM process[14], tubular geometries can be produced to achieve balloon-expandable structures[14]. The process parameters play a key role in the mechanical properties, geometrical fidelity, and surface quality. Recently the PBF-LB of NiTi stents has also been demonstrated [15][16]. It has

been shown that NiTi alloys can be used to produce variable diameters and open cell structures for patient-specific self-expandable designs [15]. The transition temperatures and initial material characterizations show promise for the superelastic behaviour obtainable. However, the mechanical characteristics of these devices are still to be developed. While studies on the mechanical properties of additively manufactured stents have been proposed [11], such works are limited to the explored stent design. As the stent manufacturing requires several steps from forming to finishing, the influence of each step on the material integrity is required to be analyzed. From this perspective fundamental works concerning the material properties for strut based biomedical devices, especially the NiTi alloys is an open field in research.

In the recent past, the attention on AM NiTi has been rapidly growing [17–19]. Especially concerning PBF-LB, several works analyzed the processability of this alloy family to investigate the shape memory effect [20,21], and superelastic properties. Different alloy compositions have been investigated studying the influence of the process parameters on the part density and the transition behaviour [22–26]. Particular attention has been paid to the manipulation of the transition behaviour via the laser process parameters [27][28] and heat treatment procedures [29][30]. Most of the proposed works cover the superelastic compressive behaviour of the PBF-LB-produced NiTi alloys, while only a few have attempted to analyze the tensile behaviour [22]. This may be related to the fact that a balance between the porosity and the transition temperature control is hard to achieve by controlling the laser process parameters. Often energy density is used to regulate the transition temperatures [31], as an increased energy density may deplete more Ni. Moreover higher energy density may induce faster solidification and cooling rates generating more precipitates and varying the Ni-Ti balance in the material matrix [32][33]. Concerning a biomedical device with micro struts ($\phi < 0.5$ mm), mechanical properties, transition temperatures, and surface roughness should all be adequate for its correct functioning in the human body [34]. This condition does not leave room for regulating all these properties via the PBF-LB process parameters. Moreover, previous works showed that for smaller features in lattice structures and strut based geometries PBF-LB process parameters are required to be selected differently [35,36]. The smaller scan tracks required for micro struts often lead to heat accumulation, increased surface roughness and geometrical deviations as well as porosity [37]. For a heat sensitive alloy such as NiTi, a size effect already seen in other alloys is expected to be much higher [38–40]. Hence, the study of a manufacturing cycle that allows obtaining adequate densification and surface roughness after PBF-LB, which can be improved via consecutive heat treatments and surface finishing operations appears as a valid route for the patient specific strut based biomedical devices.

While for PBF-LB-produced parts heat treatments and finishing operations are still under development [41], conventional stent manufacturing has established solutions. Conventionally NiTi microtubes are laser cut, heat treated, and chemically etched to retain the desired mechanical properties and surface finish [42]. Although laser cutting of stents may involve a thermal interaction with the material, its extent is limited in terms of the heat-affected zone, and the irregular cut kerf to be improved [43]. In PBF-LB, the material is fused layer-by-layer in an inert atmosphere. Hence, the chemical etching process may not be selective on the more oxidized region as it occurs with laser-cut kerf [44]. In laser-cut NiTi stents, heat treatments are often used for shape settings [45]. In PBF-LB-produced NiTi, heat treatments will be required to adjust the mechanical properties starting from a rapid solidification microstructure. All of these factors point out the fact that a fundamental study on the additive manufacturing cycle of NiTi struts is required. As a matter of fact, to the authors' knowledge tensile superplastic behavior of additively manufactured NiTi in micro struts has not been presented in the literature previously.

Biomedical applications are enabled through complete manufacturing chains that can achieve the designated functions of the device. From this perspective additive manufacturing and in particular, PBF-LB can provide the patient-specific form for cardiovascular stents. Accordingly, this work assesses a manufacturing cycle incorporating additive manufacturing, heat treatment, and surface finishing that provides the superplastic behavior to NiTi micro struts. These micro struts are the building block for superplastic cardiovascular devices, which can be produced with patient-specific designs thanks to the provided production cycle. The PBF-LB process was studied with an industrial system using pulsed wave (PW) emission varying

all laser and scan-related parameters. Heat treatment was applied at varying temperatures and hold times. Chemical etching was employed at variable durations. At each stage surface quality, geometrical deviations, and mechanical properties were assessed. The results show adequate superelastic tensile behaviour at the end of the manufacturing cycle.

2. Materials and methods

2.1. NiTi powder

The NiTi powder was produced through gas atomization and its nominal chemical composition was $\text{Ni}_{50.8}\text{Ti}_{49.2}$ (SAES Getters SpA, Lainate, Italy). Impurities were kept below 0.061 wt% C and 0.125 wt% O. The nominal particle size distribution was 15-53 μm (D10-D90). The powder had an austenite finish temperature (A_f) of 16 °C. The oxygen content of the present feedstock may be higher than that allowed for the biomedical applications [46]. At this stage of the research, it was deemed feasible as it provided adequate Ni/Ti ratio and particle distribution to assess the manufacturing cycle.

2.2. Laser powder bed fusion system

An industrial PBF-LB system (Renishaw AM250, Stone, UK) was used for this work. The system is equipped with a 200W single-mode fibre laser (R4, SPI, Southampton, UK) with 1070 nm wavelength and an optical chain that provides a 75 μm beam diameter in the focus position. The laser source is run in pulsed mode (PW) by power modulation to achieve μs -long pulses. The system works under a controlled atmosphere. Before the build process, the chamber is filled with Ar, with 15 mbar over-pressure, and during the process, the oxygen content is maintained below 1000ppm. All the experiments were carried out without any preheating of the substrate. A Reduced Build Volume (RBV) platform was installed in the PBF-LB system, which limits the build chamber to $78 \times 78 \times 50 \text{mm}^3$ while employing a limited quantity of powder (< 3kg). The melting of the powder bed was achieved by emitting a certain peak power (P_{peak}) for a fixed pulse duration (t_{on}). Layer thickness (l_z) was set constant during each build job and equal to 30 μm . The focal position was set to have the minimum beam size on the powder bed surface ($f=0\text{mm}$). On a scanning line, points exposed to the laser were separated by a given point distance (d_p), while different scanning lines were at a given line distance (d_l). Two scanning strategies were used: concentric in which the scanning lines approximate the contour of the scanned layer and meander, in which scanning lines are parallel and rectilinear segments [38]. The build jobs were prepared using Materialise Magics software (Materialise NV, Leuven, Belgium), which allows the placement of components on the baseplate area, performing the slicing phase, and assigning process parameters. The parts were loaded in the software environment in STL format.

2.3. Experimental plan

2.3.1. Selection of PBF-LB parameters

PBF-LB process parameters were studied through an extensive experimental campaign, which was specifically designed for the production of micro struts suited to stent application. Process parameter selection was based on previous works investigating the manufacturing of micro lattices and stents [9,35,47,48]. Fixed and varied process parameters are reported in Table 1. Fixed factors were powder layer thickness, sample geometry and dimensions, and pulse distance relative values. Chosen variable factors, instead, were the power, the exposure time, the absolute value of pulse distances, and the scanning strategy. Powder layer thickness (l_z), which cannot be changed within a building job, was set equal to 30 μm based allowing a high resolution along the build direction [38] and accommodating the powder size distribution up to the largest particle size upon the stabilization of the effective layer thickness [49]. Geometry and dimensions of the samples were chosen taking into consideration the desired final application, that is cardiovascular stents. Cylindrical micro struts with 300 μm nominal diameter, d_n were chosen for their affinity with stent struts. Micro struts were designed with 7 mm height (h) and a lattice support structure designed to ensure good anchoring to the baseplate and facilitate sample handling. Struts height was chosen considering a minimum dimension, required for later characterization analyses, and a maximum total build job height based on powder availability. Nominal

diameter refers to the dimension of the 3D model given as input to the PBF-LB build preparation software. Such dimension was chosen as a parameter instead of the real strut diameter because no beam compensation was applied, meaning that the final diameter is expected to be larger than the nominal one. Such choice was enforced by the micro dimensions of the samples, on which a beam compensation could lead to an insufficient number of pulses within a single cross-section. The other experimental factors which were held constant are the number of replicates (n), set as 5, and the ratio between line and point distance (d_l/d_p), equal to 1 to maintain a symmetrical pulses distribution within a cross-section. The waist diameter of the laser beam was kept on the powder bed surface ($f = 0$ mm) in order to employ the smallest laser beam diameter available at 75 μm . As previously stated, four process parameters were varied within the experimental design. Two different scanning strategies were used to investigate their suitability to produce thin structures with the employed NiTi powder. The selected strategies were meander, for its widespread usage in PBF-LB process, and concentric, based on results achieved on similar geometries with other metal powders [38]. Both laser power (P_{peak}) and exposure time (t_{on}) were varied on 3 levels choosing values as low as possible to limit the size of the melt pool in order to ensure high precision. Laser power was varied between 100 and 150W, while exposure time between 30 and 50 μs , since lower values were found to be instable in a previous work [48]. Point distance (d_p), hence line distance (d_l) since their ratio was fixed, was varied at 2 levels, 30 and 45 μm . The chosen micro strut diameter was hence divisible to both the chosen values of $d_p=d_l$. In the explored combinations the energy density varied between 49 J/mm³ and 278 J/mm³.

Table 1 Fixed and varied parameters of the PBF-LB experimental plan.

Fixed parameter	Value
Layer thickness, z [μm]	30
Focal position, f [mm]	0
Geometry	Cylindrical micro strut
Nominal strut diameter, d_n [μm]	300
Strut height, h [mm]	7
Line and point distance ratio, d_p/d_l	1
Number of replicates, n	5
Varied parameter	Value
Peak power, P_{peak} [W]	100; 125; 150
Point distance, d_p [μm]	30; 45
Pulse duration, t_{on} [μs]	30;40;50
Scanning strategy	Meander (M), Concentric (C)

For each strut produced with the PBF-LB process, SEM images were acquired up to 200X magnification (SEM EVO-50, Carl Zeiss, Oberkochen, Germany). To identify the best set of PBF-LB process parameters from the experimental design, a series of analyses were carried out, both qualitative and quantitative, the former consisting mainly in observing the successful (or unsuccessful) build of the samples. The chosen indicators to assess specimen quality were dimensional error e_d , apparent density ρ_a , and roughness indicators.

Dimensional error e_d was evaluated for each strut as the difference between measured mean diameter d_m and nominal diameter d_n :

$$e_d = d_m - d_n \quad (2)$$

Roughness was measured through focus variation microscopy (Alicona Imaging GmbH, Graz, Austria). A 5X magnification was used, with 1 μm vertical resolution and 5 μm lateral resolution. Roughness indicators were evaluated from focus variation microscope images using the ISO 4287 and 4288 standards ([50,51]). A cut-off wavelength λ_c of 0.08mm, an evaluation length L of 4mm and a total recorded distance of 6 mm were used. The following indicators were used: average roughness R_a , i.e. the average difference between peaks and valleys; RMS roughness R_q , that is the root mean square average of the profile heights over the evaluation

length; mean roughness depth R_z , i.e. the average distance between the highest peak and the lowest valley in each sampling length.

After non-destructive analyses, strut specimens were mounted in cold resin and polished to perform cross-section analyses. Cross-section optical images were acquired using Mitutoyo Quick Vision 202 Pro with a 5X objective (Mitutoyo Europe GmbH, Neuss, DE) to analyze the micro strut densification. Porosity can be generated by entrapped gases, as a consequence of vaporization due to excessive energetic input, or by lack of fusion, which happens when energy is not enough to have a complete melting of the powder [52]. The presence of porosity, which decreases the fatigue properties of the alloy ([53–55]), was observed through cross-section measurements and described by the apparent density parameter ρ_a , which can be defined with Equation 3.

$$\rho_a = \left(1 - \frac{A_{pore,tot}}{A_{tot}}\right) \cdot 100 \quad (3)$$

where $A_{pore,tot}$ is the total area of pores in a cross-section and A_{tot} is the total area of the cross-section.

2.3.2. Effect of heat treatment on mechanical properties

Heat treatment was performed on PBF-LB-processed samples to improve mechanical properties, especially in terms of superelasticity. For biomedical applications, the NiTi alloy is supposed to retain a superelastic behaviour at the body temperature (37°C). This would require the A_f to be lower than the body temperature, and the typical superelastic behaviour confirmed by tensile testing above A_f . Heat treatment was performed Ar atmosphere (SAES Getters SpA, Lainate, Italy). The samples were placed in the furnace and vacuum was applied followed by the flow of Ar filling in the furnace. Cooling was carried out in the furnace at a rate of 10°C/min. The previous work of the authors showed that a solution annealing at 850°C for 30 mins was found to be effective in ensuring A_f levels compatible with the application requirements [48]. However lower temperatures may be more favourable to the avoid grain growth and a reduction in the mechanical properties. Hence, temperature and holding time were varied aiming at an aging treatment [56]. Three levels at 450°C, 500°C, 550°C and 5 mins, 15 mins, 45 min were chosen for the temperature (T) and hold time (t) respectively. Each condition was replicated on three samples, as reported in Table 2. Both tensile specimens and differential scanning calorimetry (DSC) samples were produced with the chosen PBF-LB process parameters and then heat treated. Ad-hoc tensile specimens were designed with a 300 µm gauge diameter and 12mm gauge length (see Figure 1.a) and produced in the vertical direction. A 2D lattice geometry was chosen for DSC samples with 300 µm strut thickness and 45° inclinations (see Figure 1.b). Both tensile specimens and DSC sample dimensions were designed to be of the same order of magnitude of stent struts, to avoid possible dimensional effects on thermo-mechanical properties.

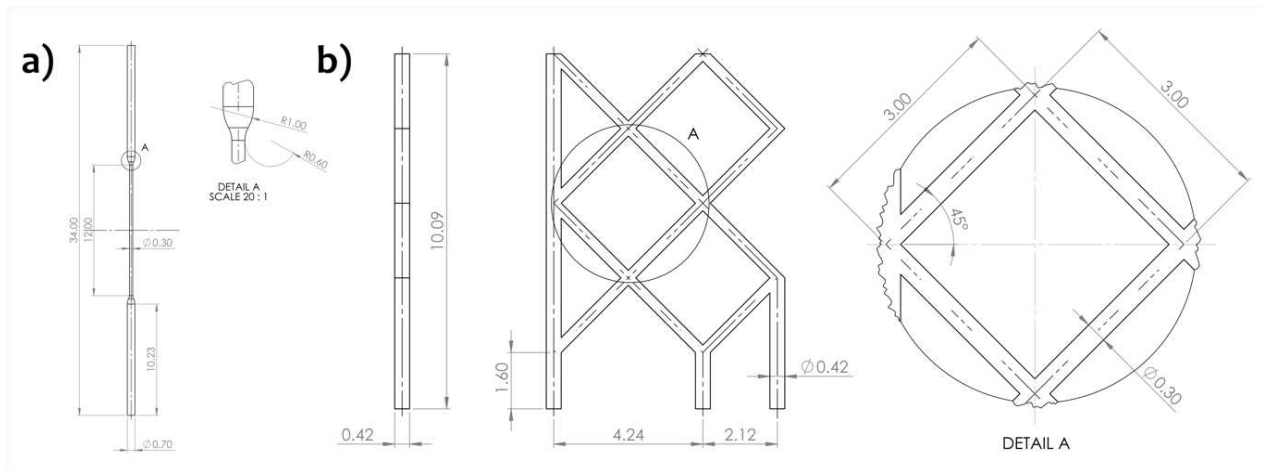


Figure 1 a) Specimen geometries for a) mechanical testing and b) DSC characterization.

Table 2 Selected parameters for the heat treatment experimental plan.

Parameter	Value
Holding time, t [min]	5; 15; 50
Temperature, T [°C]	450; 500; 550

DSC analyses were performed using Differential Scanning Calorimeter 2000 (TA Instruments, Dallas, TX), and transformation temperatures were determined following the test method described in Standard ASTM F2004 [57]. Each condition was analyzed to evaluate phase transformation temperatures and peaks. The DSC tests were performed on grid samples with an imposed variation of temperature of 10 Kmin^{-1} covering a temperature range between -160 °C and 150 °C . Three nominally identical samples were analyzed for each treatment condition. The heat flow required to heat or cool the samples was recorded as a function of temperature allowing for reconstructing the DSC plots. The DSC analysis provided the austenitic transformation peak and the martensitic transformation peak temperatures (A_p and M_p), as well as the transformation start (A_s and M_s) and finish temperatures (A_f and M_f). The start and finish temperatures of each phase transformation were calculated using tangent lines drawn in correspondence to the points where the DSC curve deviates from the baseline.

To evaluate the effect of the heat treatment on superelasticity and mechanical properties, thermo-mechanical tests were performed on the ad-hoc micro tensile specimens using MTS Synergie 200 single-column testing system with a 1 kN load cell (MTS Systems Corporation, Eden Prairie, MN, USA). The specimens were tested submerged in water and kept at 5 °C above the austenite finish temperature (A_f) in order to have a comparison between the different conditions ensuring the occurrence of austenitic transformation. In the meanwhile, for an appropriate use of the stent the test temperature should conform with the body temperature (37°C), which was considered along with the mechanical test results. For each heat treatment recipe that was studied in the present work, the austenite finish temperature for thermo-mechanical tests was chosen as the maximum obtained from DSC analyses. This approach was chosen to guarantee that the material was tested in the austenitic field to prevent the testing of a partially transformed material. Specimens were subjected to loading-unloading tensile cycles, using the ASTM F2516 [58] as a reference for the design of the test procedure. The tests consisted of pre-loading the specimen to the alignment stress (using a pre-load of 2 N), pulling the specimen to 2% strain, reversing the motion to unload the specimen to the alignment stress, pulling the specimen to 6% strain, unloading again and then pulling the specimen to failure. Dimensions of the tensile specimens were chosen to be comparable with stent struts since dependence on dimensions can be expected on the mechanical properties of PBF-LB processed materials [38]. After tensile testing, one sample belonging to each condition (as-built, heat treated and heat treated and chemically etched) was used to acquire SEM images of the fracture surfaces (SEM EVO-50, Carl Zeiss, Oberkochen, Germany).

Inductively coupled plasma mass spectrometry (ICP) was carried out on the samples at different points of the manufacturing chain consisting of PBF-LB, heat treatment, and chemical etching (HT+CE) and compared to the powder feedstock (OPTIMA 8300, PerkinElmer, Waltham, MA, USA). Inert gas fusion (IGF) was used to assess oxygen (LECO TC-436, St. Joseph, MI) and carbon (LECO CS-444, St. Joseph, MI) content at the same points in the manufacturing chain. The PBF-LB built samples were cleaned with isopropyl alcohol prior to the chemical composition measurements.

2.3.3. Surface finishing

To improve the surface quality of PBF-LB processed samples, chemical etching was performed, allowing to remove sintered particles and the staircase effect. In addition to surface quality improvement, the finishing process allowed to decrease the strut thickness. A nitric-hydrofluoric acid solution was employed, with a composition of 7 vol.% hydrofluoric acid (HF), 43 vol.% nitric acid (HNO_3), and 50 vol.% distilled water (H_2O) at room temperature. All samples were heat-treated with the chosen heat treatment condition before

chemical etching. Samples were immersed in a bath of etchant contained in a PTFE Becher. Immersion time was varied and the diameter reduction (Δd) of struts was measured following:

$$\Delta d = d_m - d_{CE} \quad (3)$$

where d_{CE} is the diameter of the strut after chemical etching. The etching time was determined and superelastic behaviour was controlled via tensile testing to verify the suitability of the finishing method.

2.3.4. Use of the determined manufacturing cycle for producing a NiTi stent mesh

In order to demonstrate the suitability of the determined manufacturing cycle for producing complex geometries for biomedical applications, a stent mesh with variable diameter was designed using a 3D wireframe approach [59]. The stent was designed with 100 μm nominal strut thickness and variable diameter as shown in Figure 2. From the top side, the stent has a starting radius that starts at 1 mm enlarging to 2 mm, then moving to 1.5 mm and finally up to 2.5 mm. The designed geometry does not refer to any specific application but highlights the advantages of the use of PBF-LB for manufacturing devices for the treatment of cardiovascular diseases in patient-specific cases requiring highly personalized solutions[60][61]. The built stent followed the determined manufacturing cycle, but its mechanical properties were not evaluated within this work. The build direction followed the axis of symmetry of the design. The built stent was using the PBF-LB process parameters, heat treatment, and chemical etching conditions providing the desired superelastic behaviour.

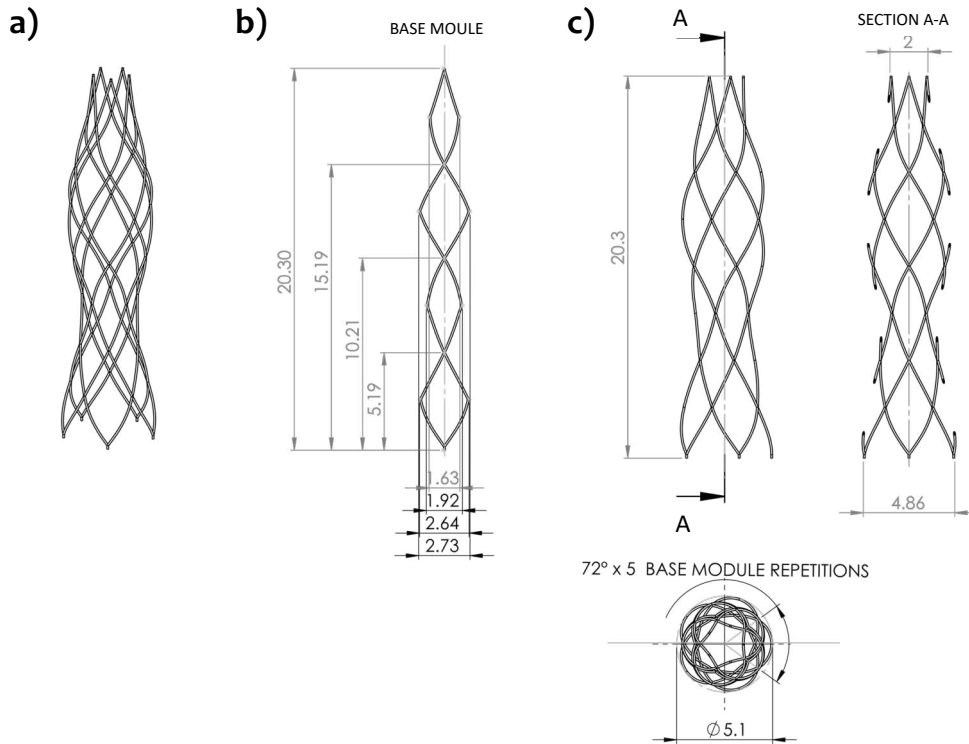


Figure 2 a) 3D view of the NiTi stent model and the technical drawings of b) unit base module and c) the produced stent mesh.

3. Results

3.1. Processability of NiTi struts by PBF-LB

All specimens were successfully built, with the only exception of all the replicates of the condition characterized by the meander scanning strategy the lowest level of all the parameters ($P = 100 \text{ W}$; $t_{on} = 30 \mu\text{s}$;

$d_p = 30 \mu\text{m}$). Figure 3 shows the struts on the substrate after the PBF-LB process, while Figure 4 shows SEM images of struts in all the processed conditions.

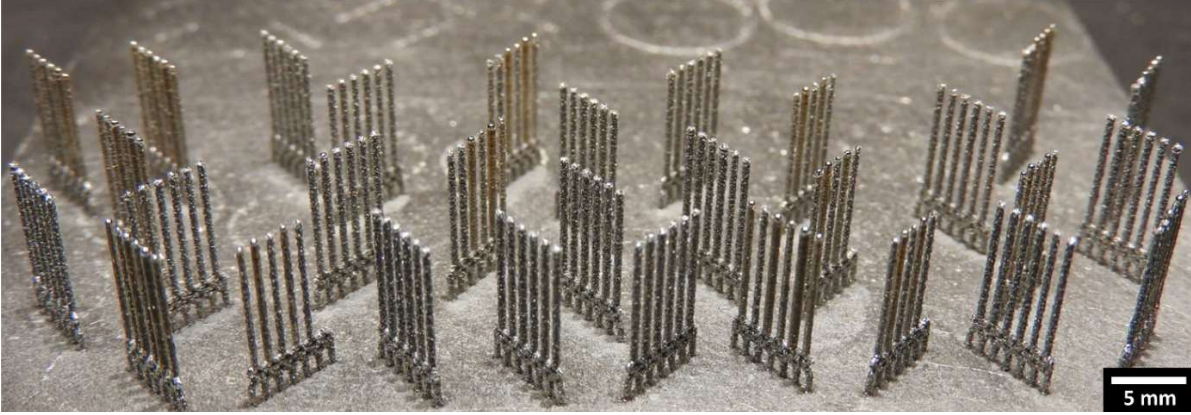


Figure 3 NiTi struts in as-built conditions on the build plate

3.1.1. Morphology

Figure 5 shows the mean diameter of the struts as a function of process parameters and it appears that the combination meander scanning strategy and $t_{on} = 30 \mu\text{s}$ gave higher thickness variation, with a minimum of $342 \mu\text{m}$ and a maximum of $595 \mu\text{m}$. With a concentric strategy, instead, it seems that no process parameter had a clear effect on thickness, and the diameters varied between $416 \mu\text{m}$ and $533 \mu\text{m}$. However, looking at SEM images reported in Figure 3.9, it is visible how the meander scanning strategy gives smoother surfaces and uniformity, while the concentric one results in a much higher amount of sintered particles on the surface, leading to a higher variation in terms of diameter along a strut axis. This effect could be explained by melt pool behavior and surface tension effects. Dimensional error for the combination meander strategy and $30 \mu\text{m}$ point distance shows an increasing trend with power ranging from $109 \mu\text{m}$ and $268 \mu\text{m}$. With a $45 \mu\text{m}$ point distance instead, no evident trend is visible, but a lower error is measured with values between $42 \mu\text{m}$ and $156 \mu\text{m}$. Regarding concentric strategy instead, a sensible trend is not visible with process parameters on the dimensional error, which maintains values in the interval $119 \mu\text{m}$ and $187 \mu\text{m}$. Figure 6 shows the mean diameter of the struts as a function of process parameters

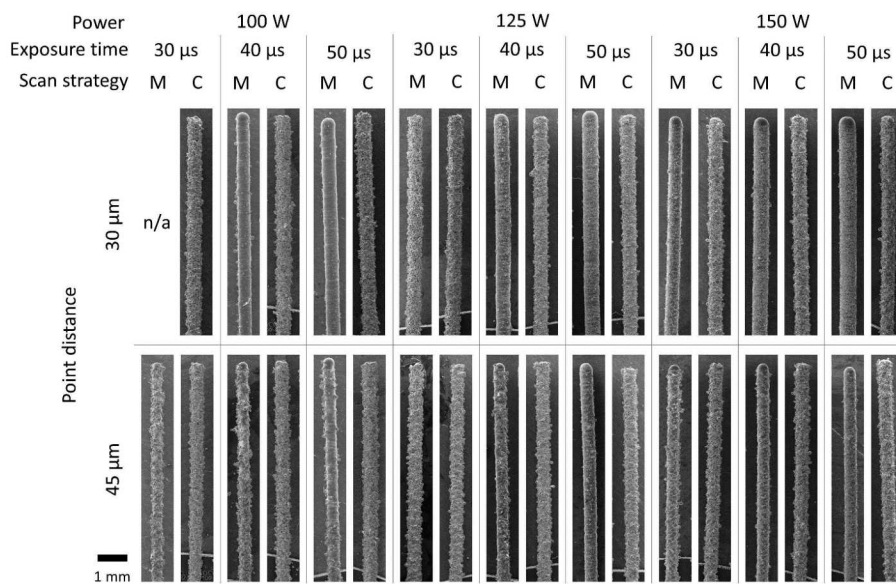


Figure 4 SEM images of NiTi struts produced with PBF-LB process (M: Meander, C: Concentric).

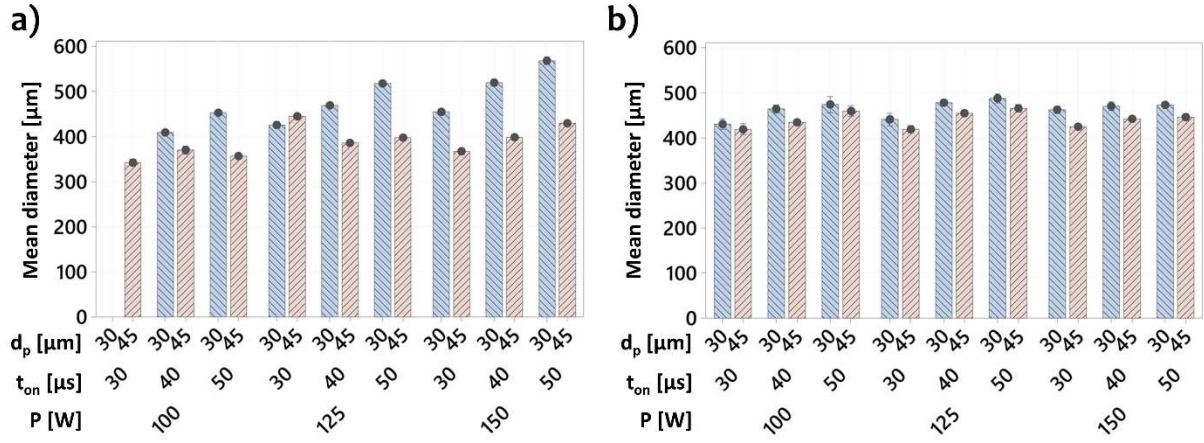


Figure 5 Mean diameter of NiTi struts (d_m) in the as-build condition as a function of PBF-LB process parameters. a) Meander and b) concentric scanning strategy. Error bars indicate one standard error from the mean.

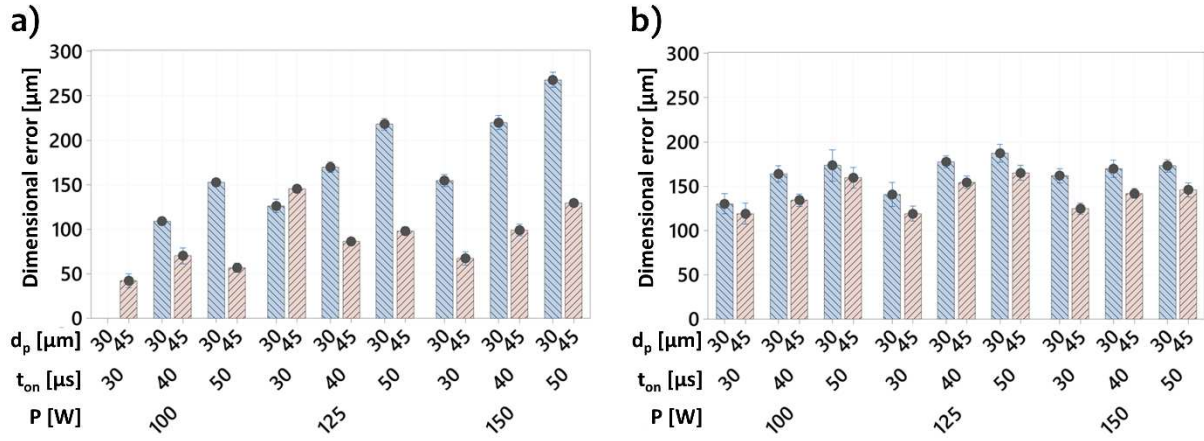


Figure 6 Dimensional error on mean diameter (e_r) of NiTi struts in the as-build condition as a function of PBF-LB process parameters. a) Meander and b) concentric scanning strategy. Error bars indicate one standard error from the mean.

3.1.2. Density

Figure 7 shows longitudinal cross-section images of struts in all the processed conditions, while Figure 8 shows the apparent density of the struts as a function of process parameters. Apparent density varied between 95.2% and 99.7% with the meander strategy, while for the concentric strategy the variation was between 93.8% and 99.6%. The best and worst density cases are also shown in enlarged images within Figure 7. It can be seen that between the two conditions the scan strategy, the exposure time change, and the point distance change. The shape of the pores in the best case is spherical indicating gas entrapment.

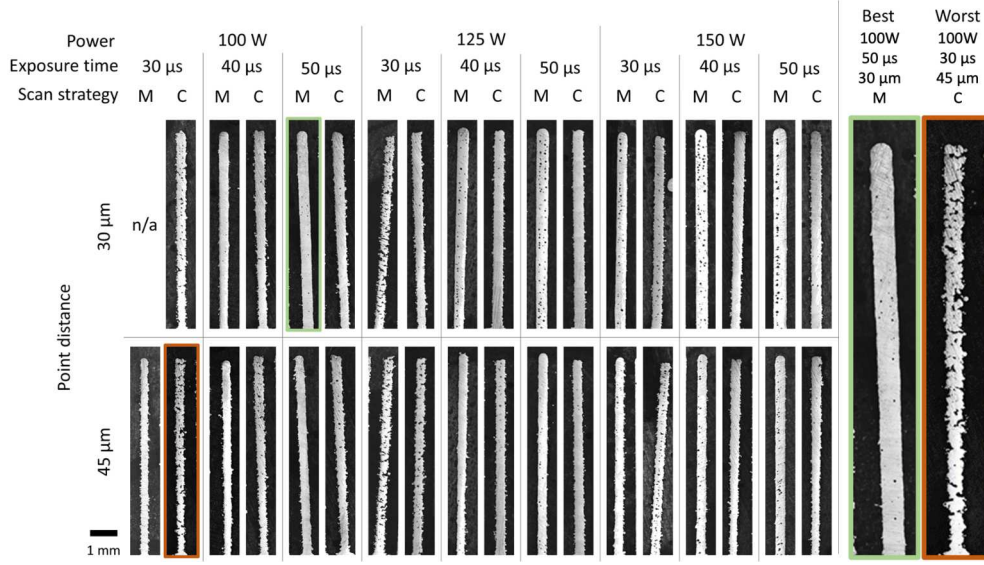


Figure 7 Cross-sections of NiTi struts produced with LPBF process (M: Meander, C: Concentric). Best and worst density conditions are shown in the insets.

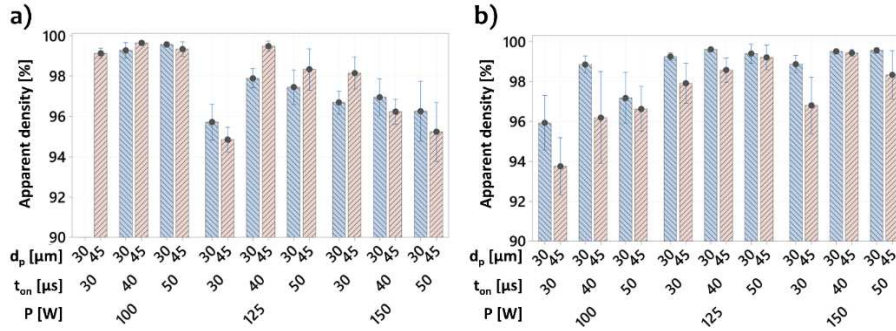


Figure 8 Apparent density (ρ_a) of NiTi struts in the as-build condition as a function of PBF-LB process parameters. a) Meander and b) concentric scanning strategy. Error bars indicate one standard error from the mean.

Figure 9 shows surface reconstructions of struts in all the processed conditions. The colourmap indicates the height difference of the primary surface profile with respect to the a common zero plane. The height maps showing a more homogenous colour distribution indicate lower surface roughness. Figure 10 shows roughness indicators of the struts as a function of process parameters. It appears that the meander scanning strategy can provide lower roughness values in comparison with the concentric one. With the latter, moreover, the effect of other process parameters seems to be absent. Using the meander strategy instead, it appears that 30 μm point distance results in lower roughness than 45 μm . In particular, R_a values varied between 3.1 μm and 18.1 μm with the meander strategy, while with the concentric strategy the interval was between 11.6 μm and 17 μm . Regarding R_q values, the measured interval was [3.9 μm , 23.4 μm] with meander strategy and [14.3 μm , 22.4 μm] with concentric strategy. For R_z , instead, intervals of [20.5 μm , 110.8 μm] and [64.9 μm , 105.9 μm] were measured for the meander and concentric strategy respectively.

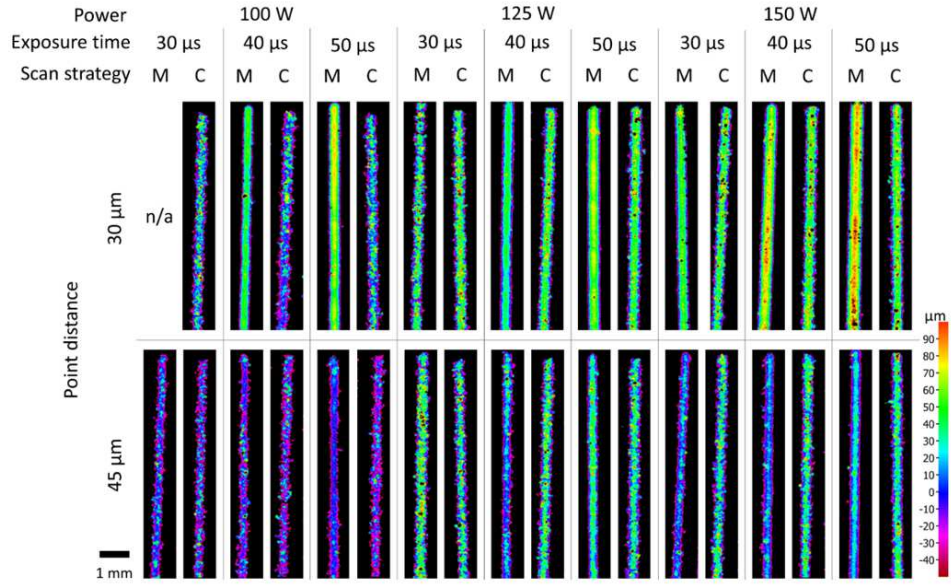


Figure 9 3D reconstruction of NiTi struts as a function of PBF-LB process parameters obtained using focus variation microscopy (M: Meander, C: Concentric).

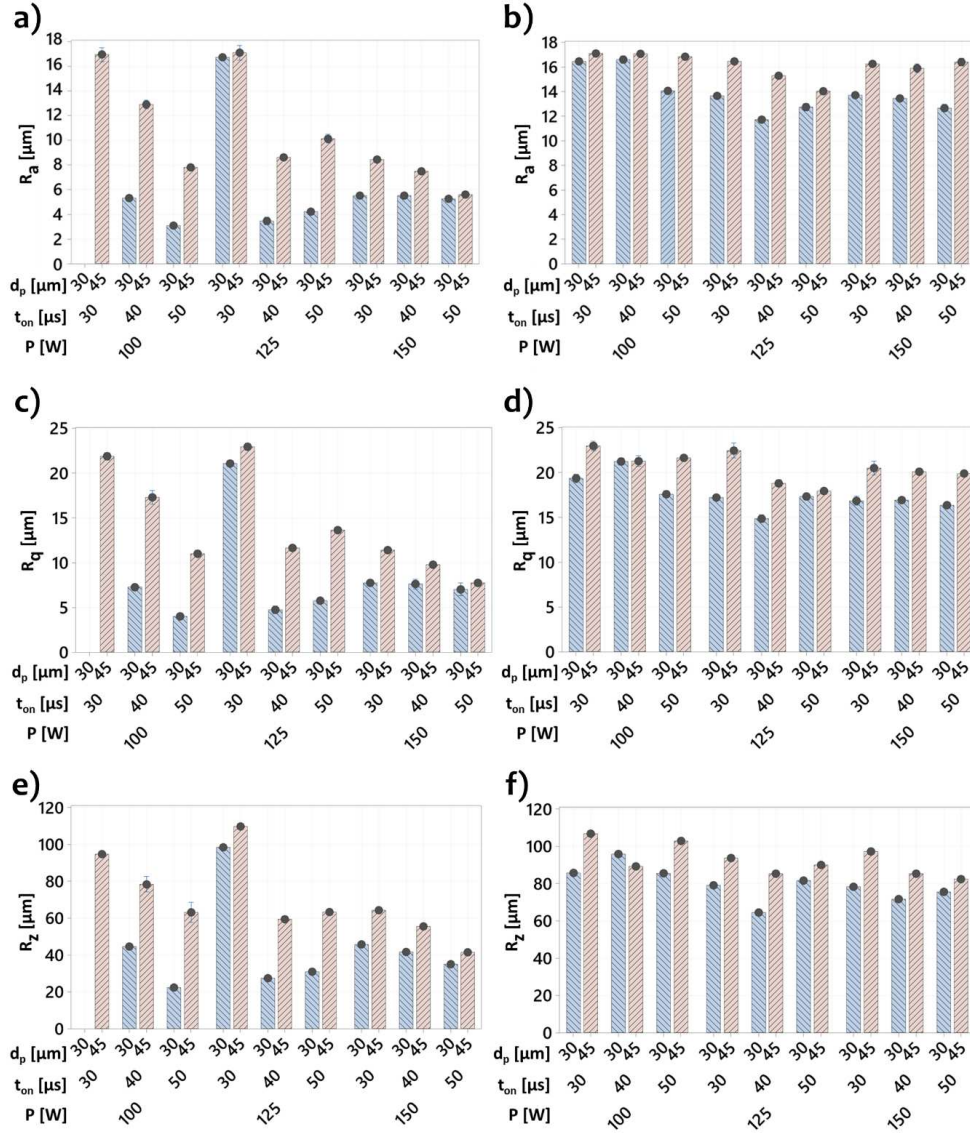


Figure 10 Roughness indicators R_a (a,b), R_q (c,d), R_z (e,f) of NiTi struts in the as-build condition as function of PBF-LB process

parameters. a,c,e) Meander and b,d,f) concentric scanning strategy. Error bars indicate one standard error from the mean.

3.1.3. Selected PBF-LB process parameters

Combining data from apparent density and roughness measurements, the following set of PBF-LB process parameters was identified: laser power $P = 100\text{W}$; exposure time $t_{on} = 50\text{ }\mu\text{s}$; pulse spacing $d_p = d_l = 30\text{ }\mu\text{m}$ and meander scanning strategy. The resultant energy density was 185 J/mm^3 . Such a set allowed to achieve $99.6\pm0.2\%$ apparent density, and average roughness $R_a=3.1\pm0.1\text{ }\mu\text{m}$, $R_q=3.9\pm0.1\text{ }\mu\text{m}$, $R_z=20.5\pm2.6\text{ }\mu\text{m}$. Regarding the mean diameter of the strut, a value of $453 \pm 11\text{ }\mu\text{m}$ was measured with a dimensional error corresponding to 51% of the nominal diameter. SEM images, cross-section, and surface reconstruction of a strut produced with the identified set of process parameters are shown in Figure 11.

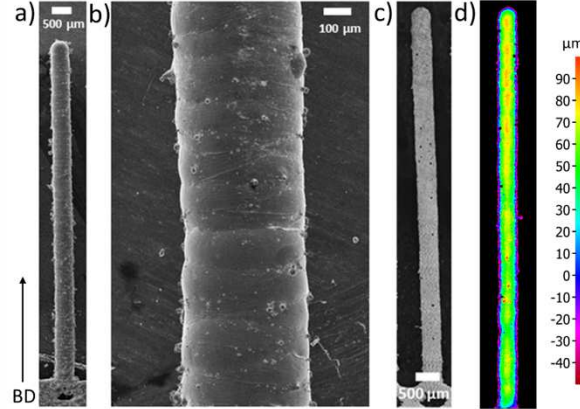


Figure 11 a) SEM image with a b) detail, c) cross-section and d) surface reconstruction of a strut produced with the identified set of PBF-LB process parameters ($P = 100\text{W}$; $t_{on} = 50\text{ }\mu\text{s}$; $d_p = d_l = 30\text{ }\mu\text{m}$; meander scanning strategy).

Further analyses concerning the transformation behaviour, heat treatment, and chemical etching studies as well as mechanical testing were applied employing the parameter set.

3.2. Thermo-mechanical properties

3.2.1. Transformation temperatures

DSC analyses of NiTi powder and as-built samples produced with the chosen parameter set are reported in Figure 12. For the powder, the DSC plot showed low and wide transformation peaks, while in the as-built state a baseline was not evident. Start and finish transformation temperatures for the as-built condition were difficult to identify, but peak values can be defined. In particular, austenite peak temperature A_p had a mean value equal to $20.5\text{ }^\circ\text{C}$ with a standard deviation of $10.6\text{ }^\circ\text{C}$ on three replicate samples, showing a high variation among different specimens. Instead, martensite peak temperature M_p had a mean value equal to $-10.3\text{ }^\circ\text{C}$ with a standard deviation of $0.6\text{ }^\circ\text{C}$.

In Figure 13, DSC plots of the heat-treated specimens are shown, as a function of temperature and holding time. The peak along the heating curve identifies the endothermic transformation between the martensitic phase of the NiTi alloy and the austenitic one, while the peak along the cooling curve identifies the reversed transformation, which is an exothermic transformation. It seems that at low temperature ($450\text{ }^\circ\text{C}$) the transformation from martensite to austenite upon heating has narrower and higher peaks, meaning that higher energy is required, and start and finish temperatures are close to each other. Moreover, with increasing temperature, the R-phase [62] which appears in the cooling phase tends to disappear. Figure 14 shows how transformation temperatures vary with different heat treatment parameters. It appears that austenite start temperature A_s becomes negative when treated at $550\text{ }^\circ\text{C}$, while martensite start temperature M_s becomes positive. Moreover, it seems that the latter increases with time. Both transformations seem to have a peak temperature increasing with holding time, with values always positive for the austenite and negative for the martensite transition. In almost all the heat treatment conditions, it can be found that peak temperatures are

lower than the ones for as-built specimens. Finally, for finish temperature, lower variations were found in comparison with the other transformation temperatures and the martensite finish temperature had a low variability with temperature.

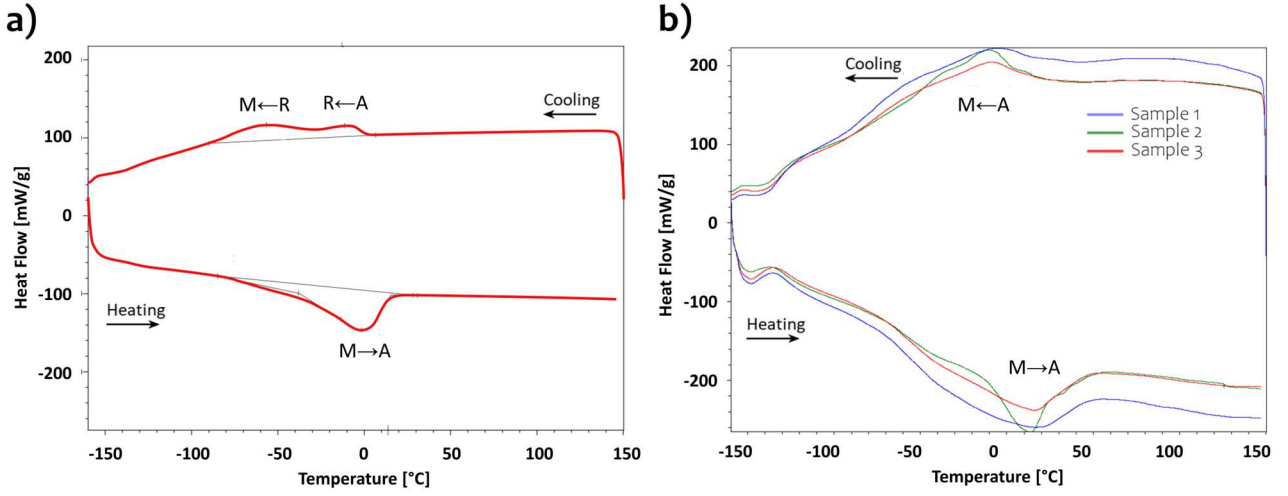


Figure 12 DSC plots of a) NiTi powder and b) as-built samples produced with the PBF-LB process.

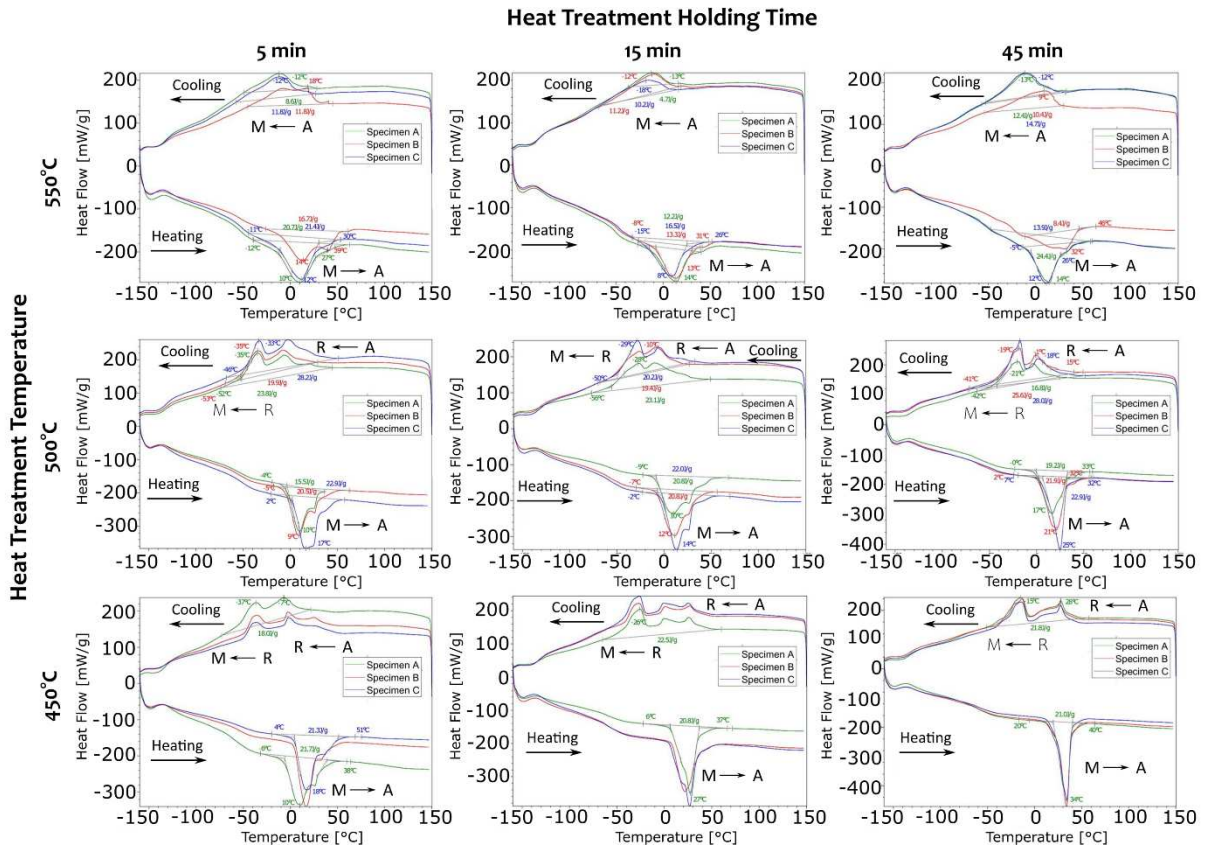


Figure 13 DSC plots of heat-treated specimens as a function of holding time and temperature.

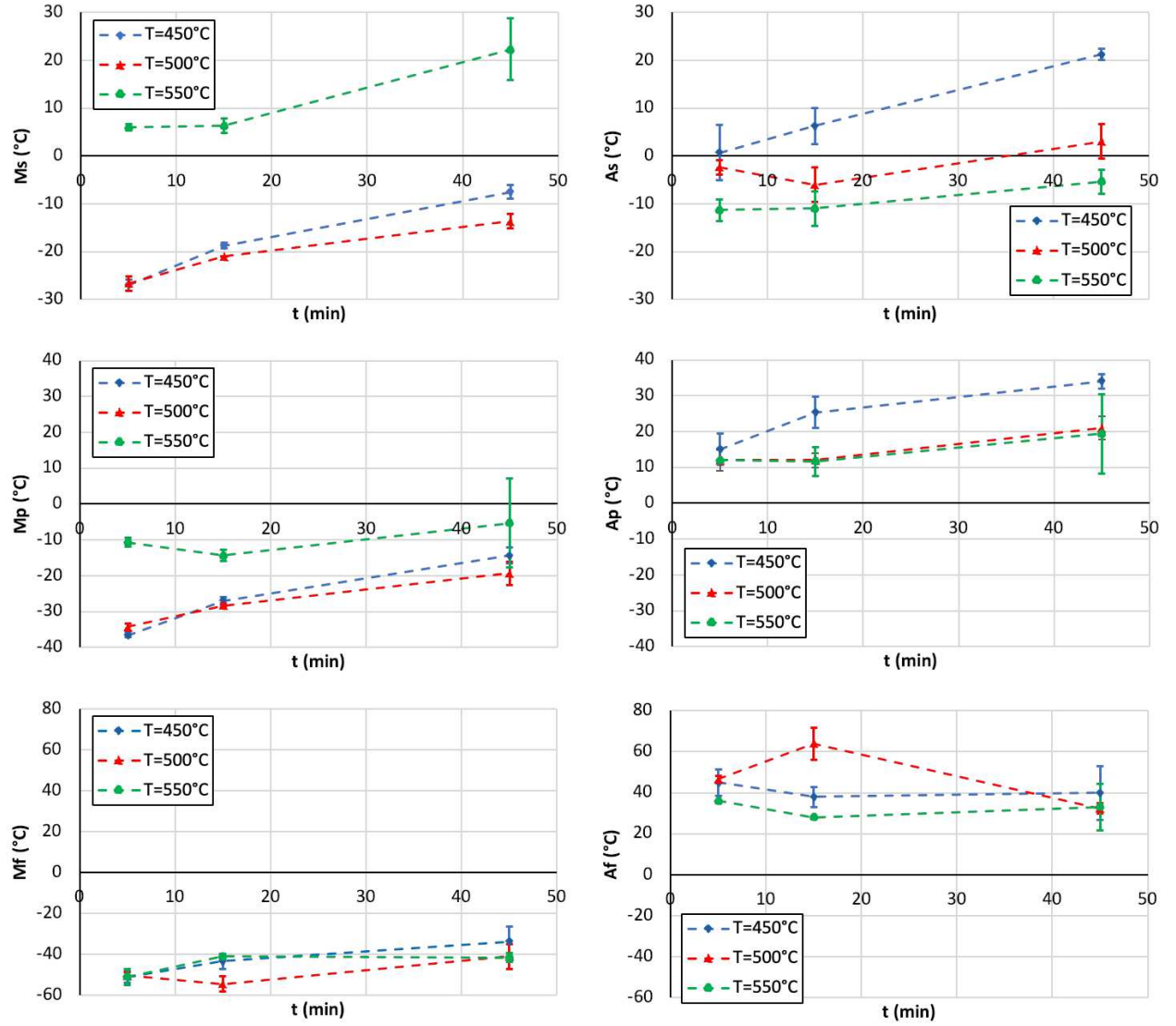


Figure 14 Transformation temperatures of the NiTi alloy produced by PBF-LB as a function of heat treatment parameters. a) Austenite (A_s) and b) martensite start (M_s) temperatures; c) austenite (A_p) and d) martensite peak (M_p) temperatures; e) Austenite (A_f) and f) martensite finish (M_f) temperatures. Error bars represent standard error and dashed lines depict trend only.

3.2.2. Superelastic behaviour of heat-treated samples

As-built specimens showed high fragility and low repeatability, where one specimen failed at the first cycle, while the other two tested specimens failed during the second loading cycle. In Figure 15, stress-strain curves of the heat-treated tensile specimens are shown, as a function of temperature and holding time. With a 450 °C temperature, there was a slight improvement in the first tensile loading, but the specimens still reached fracture before the first unloading. Considering higher temperature and 5 min holding time, two specimens reached failure during the second loading. Instead with 500 °C and 550 °C temperatures and 45 min holding time, there is a slight presence of the second loading-unloading cycle. The better results in terms of superelasticity were reached with 500 °C and 550 °C temperatures and 15 min in which failure was reached during the final loading step. It appears that the combination of 550 °C and 15 min gives the best results in terms of both superelasticity and repeatability, with all three tested specimens reaching fracture during the final loading, elongation at fracture of 5.4%, maximum stress of 705 MPa, and austenite finish A_f temperature of 28.0 ± 2.7 °C, which guarantees to have the material in the austenitic phase at body temperature (37°C).

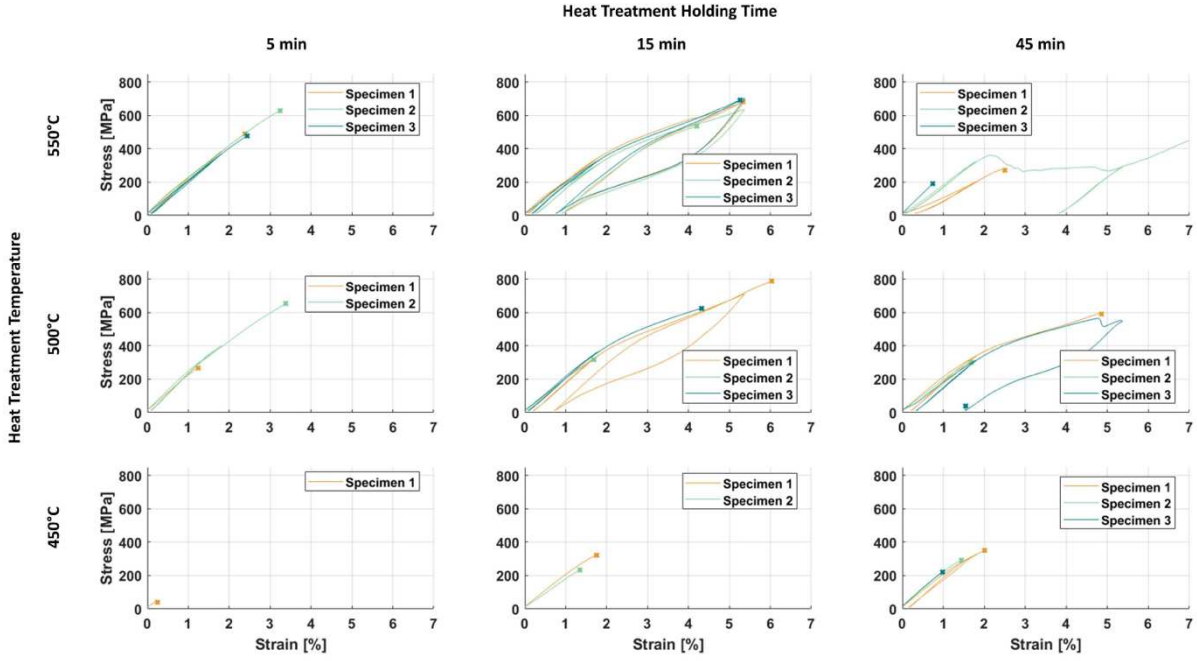


Figure 15 Stress-strain curves of the NiTi tensile specimens produced with PBF-LB process, heat treated, and subjected to loading-unloading cycles.

3.3. Influence of chemical etching on surface finish and superelastic behaviour

Results of diameter reduction (Δd) on struts after chemical etching are reported in Figure 16. Varying time from 8 minutes to 15 minutes, diameter reduction varied in the interval of 47 μm to 157 μm . After 14 minutes all the sintered particles were removed and a smoother surface finish was achieved. The results show that the chemical etching operation starts with the immediate removal of the sintered particles and then the layered structure of the surface. A homogenous surface can be achieved at approximately 10 min level. Further etching can be used for regulating the strut thickness. Figure 17 shows SEM images of a chemically etched strut specimen after 14 minutes of immersion. The strut had a nominal diameter of 300 μm , while the as-built diameter was 445 μm , which was reduced to 330 μm after chemical etching. The chemical etching could reduce the R_a of the employed specimens by $23 \pm 1\%$. While the layered structure of the surface, as well as the sintered particles, could be removed, the surface topography showed signs of local pitting. The use of a less aggressive etchant with a prolonged chemical etching duration may be a relevant solution.

Figure 18 compares the tensile behaviour of as-built, heat-treated, heat-treated, and consecutively chemically etched samples. It can be seen that similar superelastic behaviour can be maintained after chemical etching indicating that the finishing process is not expected to have a significant effect on the mechanical behaviour.

Table 3 collects the chemical composition measurements carried out with ICP and IGS methods. It can be seen that Ni depletion appears to be evident after the PBF-LB process and heat treatment, which is also accompanied by an increase in the C and O content. After the heat treatment the O content appears to slightly increase. After the chemical etching phase the C and O contents appear to be reduced along with a recovery of the Ni content. Considering the tensile behaviour at the different processing points the role of chemistry can be further analysed. It is expected that the heat treatment provides the dissolution of precipitates back to the matrix ensuring an overall improved mechanical behaviour. Upon the chemical etching phase, the removal of Ti-oxides is expected compensate for the Ni depleted during the PBF-LB process. Moreover, chemical etching removes surface imperfections and the fragile surface oxides that can lead to the relatively lower ultimate tensile stress observed. The combined effect of heat treatment and chemical etching is expected to provide the final superelastic behaviour.

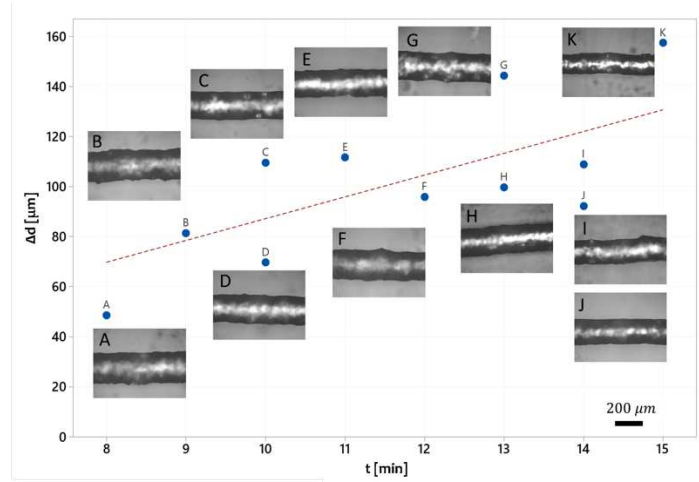


Figure 16 Diameter reduction as a function of immersion time for chemically etched NiTi struts. An optical image after the etching process is shown for each sample denoted with their letters (A-K). The dashed line depicts the trend only.

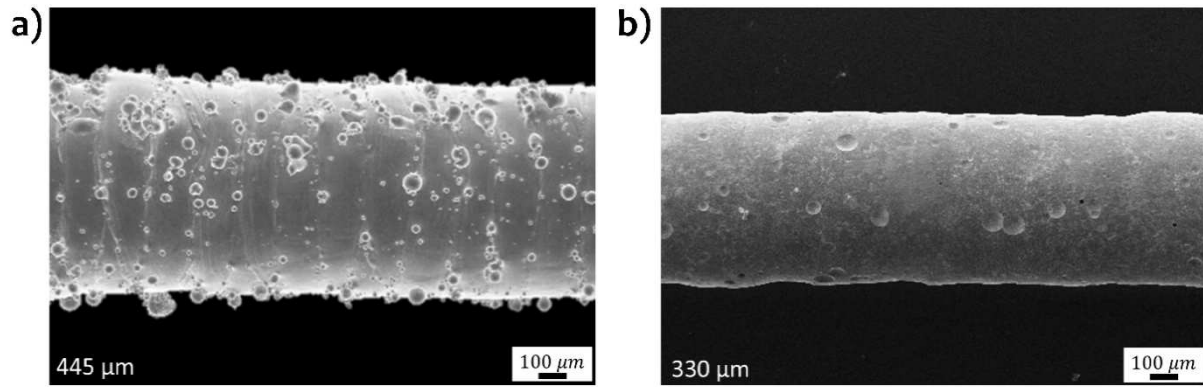


Figure 17 SEM images of a) an as-built strut with 445 μm diameter and b) the same strut after chemical etching with a final diameter of 330 μm .

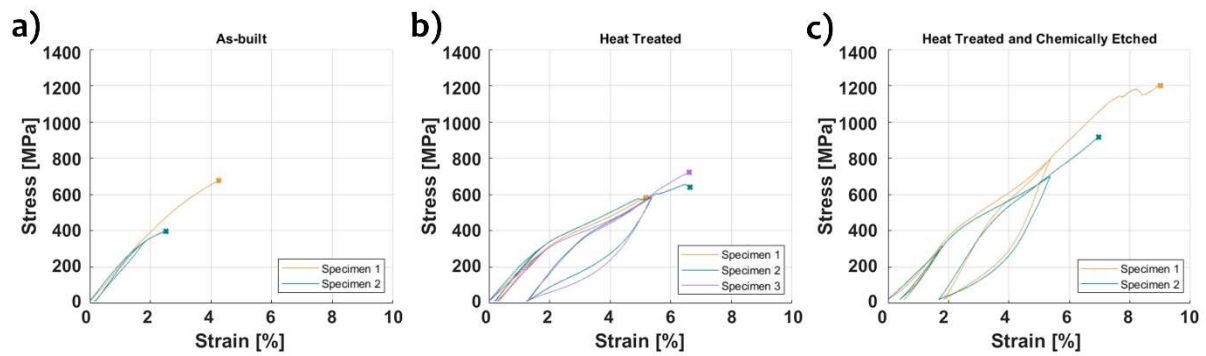


Figure 18 Stress-strain curves of the NiTi tensile specimens produced with PBF-LB process and subjected to loading-unloading cycles in a) as-built condition, b) after heat treatment at 550°C for 15 minutes and c) after both heat treatment and chemical etching.

Table 3 Chemical composition measurements of the materials at different processing conditions (HT: Heat treatment, CE: Chemical etching).

Condition	NiTi at%	C wt%	O wt%
Powder	Ni _{50.8} Ti _{49.2}	0.061	0.125
As-built	Ni _{50.2} Ti _{49.8}	0.073	0.180
HT	Ni _{50.1} Ti _{49.9}	0.076	0.199
HT+CE	Ni _{51.1} Ti _{48.9}	0.049	0.156

3.4. Fracture surfaces

All the analyzed samples exhibit fractures in the gauge length. The analysis of the fracture surfaces is shown in Figure 20. In all cases, inclusions are not detected. Presence of spherical pores indicating local vapour entrapment is visible. Pores around the sample borders are more accentuated in the as-built (Figure 20.a) and less accentuated in the heat treated (Figure 20.c). Higher magnifications (Figure 20.b, d, f) show the absence of clear signs of ductile failure in the material.

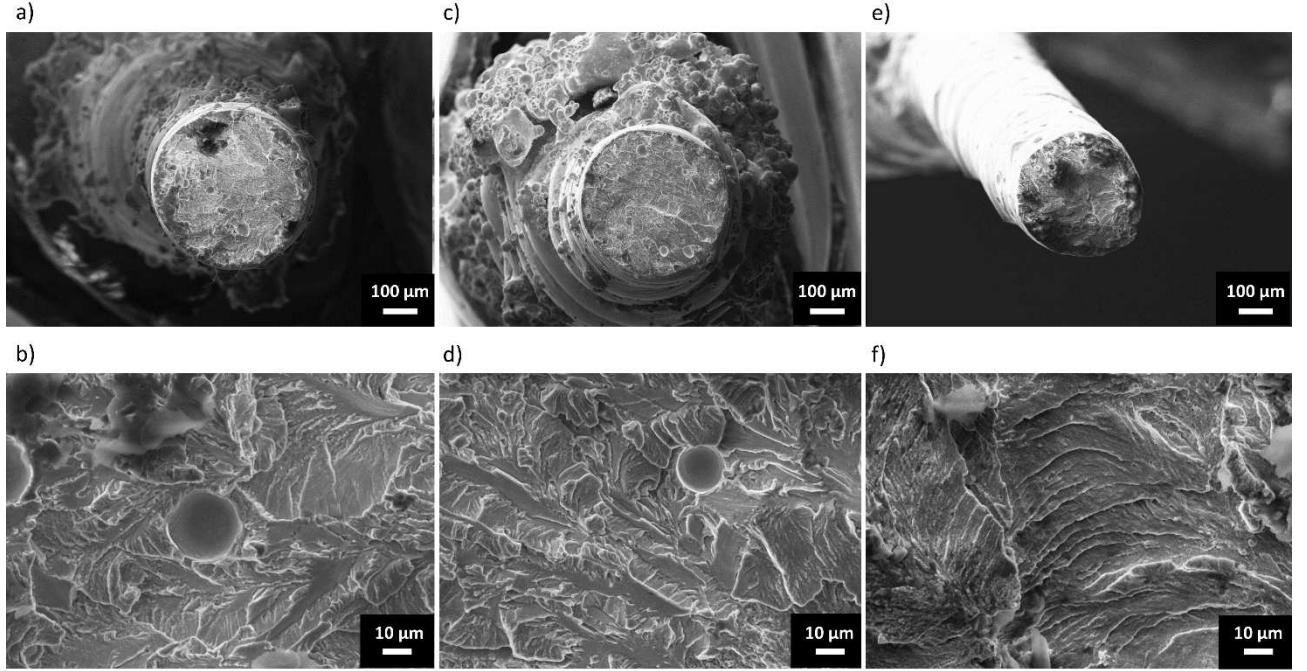


Figure 20 SEM acquisitions of the fracture surfaces after tensile testing of one of the as-built (a, b), heat treated (c, d) and heat treated and chemically etched (e, f) samples at lower (a,c,e) and higher magnifications (b,d,f).

3.5. Additive manufacturing of a stent mesh

Figure shows SEM images of the manufactured NiTi stent meshes in as-built and post-processed conditions. The stents were manufactured using parameters the chosen PBF-LB parameter ($P = 100\text{W}$; $t_{on} = 50\text{ }\mu\text{s}$; $d_p = d_l = 30\text{ }\mu\text{m}$; meander scanning strategy), followed by a heat treatment of 500°C for 15 mins, and chemical etching for 10 mins. The images show that the employed PBF-LB strategy is capable of producing thin struts even at $100\text{ }\mu\text{m}$ nominal diameter. The surface topography in the as-built condition shows sintered particles and traces of the staircase effect. After the post-processing steps including chemical etching, the surface is free of sintered particles and a reduction of the diameter is observed. The strut diameter was measured at $184\pm 14\text{ }\mu\text{m}$ in as-built condition and $129\pm 8\text{ }\mu\text{m}$ after the post-processing operations.

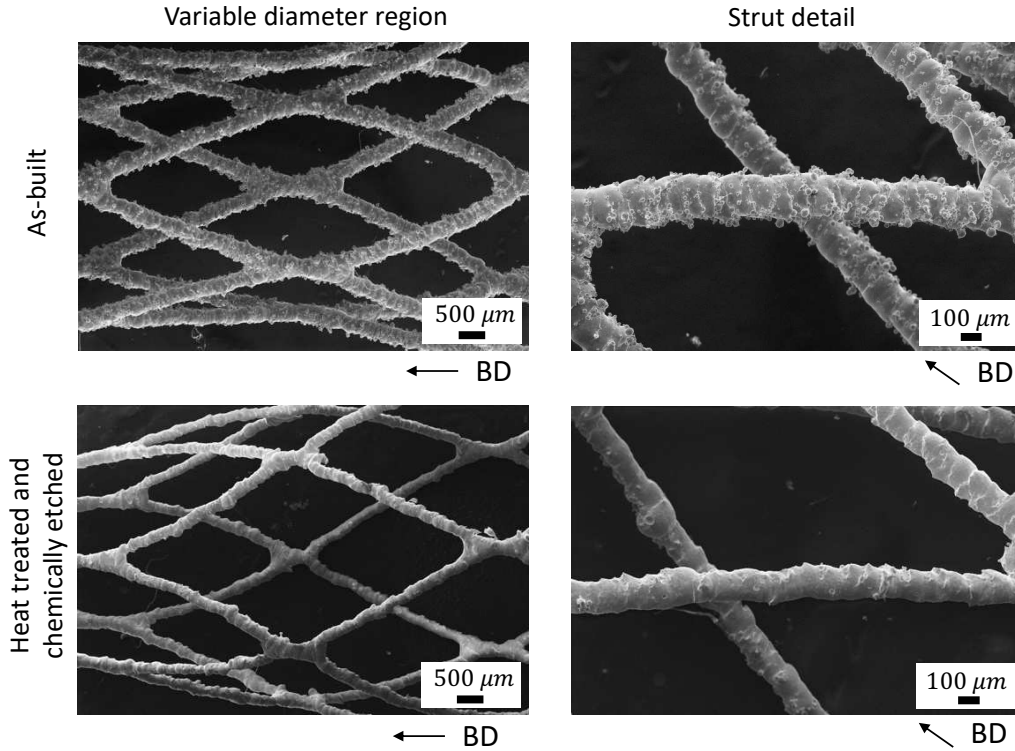


Figure 21 SEM images of the NiTi stent mesh with variable diameter in as-built condition and after the post-processing operations. (BD: Build direction).

4. Discussion

For a cardiovascular NiTi device, the fundamental requirements are related to the mechanical behaviour in static and fatigue conditions combined with the surface finish. Indeed, the functionality of the device, which passes through superelastic behavior at body temperature and repeated applied loads, is obtained through the correct manufacturing cycle that involves feedstock, shaping, and finishing operations. In literature, several works have attempted to regulate the transition temperatures and the mechanical properties of PBF-LB processed NiTi alloys. While for larger components, this may provide a valuable solution, for micro struts to be used in biomedical applications, the process window is very small for such variations. The results showed that an overall compromise between density, geometrical integrity, and surface roughness exists when choosing PBF-LB process parameters. The following heat treatment and chemical etching steps indeed require adequate initial conditions (i.e. high density and low surface roughness) to provide significant improvements.

Being a highly sensitive material to chemical and thermal variations, at each step, NiTi alloys undergo a remarked change. Often the conventional manufacturing cycle is optimized for the given geometry and the function of the single device. In the case of additively manufactured, patient-specific NiTi alloys such changes pose a wider challenge. Although not studied here in detail, the chemistry of the feedstock produced through powder atomization is a key aspect to maintain the Ni-Ti balance in the final product. While several works in the literature investigated the Ni losses in the PBF-LB operation, commercial availability of NiTi powders with stable powder chemistry and size distribution is still scarce [63,64]. While the more accurate chemical composition characterization was not the main focus of this work, the results showed that the micro struts produced had an alteration with respect to the initial $\text{Ni}_{50.8}\text{Ti}_{49.2}$ composition. In as-built struts produced with the chosen process parameter combinations, the increased O and C content may reduce the alloying elements from the matrix, while the overall Ni/Ti proportion appeared to be stable. The higher as-built transition temperatures, especially A_f suggest that the Ni content in the matrix was reduced. Ni depletion can occur during the process due to its lower vaporization temperature. A lower Ni content can lead to a rise of A_f [65]. The

presence of spherical pores found in the cross-sections can be an indicator to such depletion. In the chosen PBF-LB process parameter combinations, the pore amount was also very limited. On the other hand, the rise of A_f in the as-built condition may depend on the decrease of Ni in the matrix due to precipitation formation [66]. The role of the heat treatment is expected to dissolve the precipitates and increase the Ni content in the matrix as the transition temperatures are reduced with respect to the as-built condition. Indeed a deeper inspection of the material chemistry, microstructure, along with process defects is required to ensure the desired fatigue properties. The chemical composition, the generated phases and the possible generation of Ti_xNi_y precipitates would be required to assess in the powder form, in as-built and heat treated conditions. A greater understanding of these features will enhance the manufacturing route selecting the more appropriate feedstock, process and heat treatment parameters.

The mechanical properties obtained at each step of the manufacturing chain provide further insights. The work underlined the importance of the process parameter selection in PBF-LB for the reduction of pores. The pore shape in the worst case is irregular, indicative defects due to lack-of-fusion. Such difference in apparent density can be attributed mainly to the reduction in energy density by 40%. It can also be expected from the overall trend in the density results that the meander scan strategy may induce a low with a scan strategy that apparently induce higher heat accumulation in the limited sizes of the micro struts. Indeed with conditions corresponding to higher energy input with higher power, higher exposure time and lower point distance, the apparent density of micro struts produced with meander scan strategy have lower apparent density due to vapour entrapment observed in the form of spherical pores. Instead the same highly energetic conditions allow to reach higher apparent density when concentric scan strategy is used.

The work showed that adequate density and surface roughness could be achieved in PBF-LB, while the previously unreported superelastic behaviour in this dimensional range was achievable through heat treatment. In the case of micro struts, the efficacy of using PBF-LB as the main forming process while using heat treatments for adjusting the mechanical properties has been confirmed. The fragile behaviour in the as-built condition without the presence of excessive porosity can point to the abundance of brittle precipitates in the material. The heat treatment helps dissolve these precipitates in the matrix and provides conditions for superelasticity. The effect of chemical etching appears remove the surface oxides, improve the NiTi ratio, maintain the superelastic behaviour, while the maximum strength at rupture is increased. This can be attributed to a more homogenous surface finish allowing to avoid the influence of a reduction in the local section. The surface finishing eliminates the sub-surface defect area that is present in the as-built and heat-treated samples (Figure 20.a, c). From the observation of the fracture surfaces, it is possible to state that brittle failure is occurring in each sample. This has been already reported in the literature on PBF-LB aluminum or titanium alloys, compared to the traditionally manufactured counterparts [67][68]. Although operating under inert atmosphere, during the PBF-LB oxygen remains in the build chamber. The oxygen presence may induce a fragile fracture as observed in the Ti-alloys [69]. In addition to the sub-surface defects the presence of oxides is expected to contribute to the highly brittle fracture observed in the as-built specimens. The chemical etching is expected to contribute also by removing surface oxides reducing the fragility. However, as oxygen is also expected to be retained in the material bulk contributing to the brittle failure behaviour observed in the fracture surfaces. Concerning the mechanical properties of the PBF-LB-built parts, anisotropy is known to be an issue [70]. Commonly, tensile tests are carried out with specimens oriented in different directions with respect to the build direction. The vertical build direction is expected to be the weakest since the forces are applied normally to the layering direction. However, during the production of complex geometries such as stents, the heat accumulation may differ according to the scanned layer, which can affect the local material properties. The role of heat treatments and chemical etching operations as homogenizing processes is further highlighted by considering such variations.

With the data gathered in this work, mechanical properties can be simulated in finite element modelling (FEM) frameworks. For patient-specific biomedical devices, FEM platforms are expected to be the key to future applications[71]. While the manufacturing chain can be certified at each stage as shown in this work, the certification of every single implant will require the use of digital means. Indeed, the same device can be

produced for only testing purposes before implantation. The limiting factor in such a situation would not be the production cost, but the implantation time. From this perspective, topological optimization, in-silico testing, and certification of each device design will be fundamental. Modular designs and the use of universal design criteria are among the subjects that will require further attention. Indeed, the simulated functions can be expected to be valid, if the manufacturing stability can be retained. The demonstrator case confirmed the transferability of the manufacturing cycle to complex stent geometries. However, with variable designs the occurrence of process variations may be more likely. Hence, in-situ process monitoring of the PBF-LB should also be focused on chemical variation, as well as more commonly addressed issues such as porosity and geometrical deviations.

5. Conclusions

This work studied a complete manufacturing cycle of NiTi micro struts for biomedical device applications. In particular, the PBF-LB of $\text{Ni}_{50.8}\text{Ti}_{49.2}$ powder was studied identifying the variations of transition temperatures and dimensions after heat treatment and chemical etching. The main achievement of the work has been the demonstration of tensile superelasticity in micro struts in operating conditions compatible with the body temperature. The other main outcomes of the work can be summarized as follows.

- High-quality micro struts in NiTi could be produced via PBF-LB considering both laser emission and scan strategy-related parameters. The small dimensions of the struts required the spatial PBF-LB parameters to be matched to the strut size along with the scan strategy.
- The best PBF-LB conditions could provide high density and low surface roughness together, which are found to be highly desirable for the successive heat treatment and chemical etching phases. On the other hand, the mechanical properties and the transition behaviour of the as-built PBF-LB micro NiTi struts were far from ideal.
- The heat treatment could be applied at relatively moderate temperatures and durations (ie. 500°C , 15 min), which provided the desired superelastic behaviour at tensile testing conditions with A_f below the body temperature.
- The chemical etching removed the sintered particles and the layered structure of the surface, providing a more homogenous finish. It was seen that this phase can be used both for a reduction in the thickness and the surface roughness.
- The overall production cycle provided superelastic tensile behaviour with micro struts previously not reported in the literature. The superelastic behaviour was observed with strain levels up to 5% and retained plasticity of below 2%.
- The present results show high compatibility with stenting applications in terms of tensile properties, transition temperatures, and surface finish. On the other hand, the fatigue properties and finite element modelling aspects require further attention.
- The proposed production cycle was effectively used for producing complex stent meshes. The results show transferability from the building blocks towards the final medical device through the systematic investigation of the involved process parameters.

The present work provided both the validation of a complete manufacturing cycle as well as data concerning the material properties. An important aspect of the work that requires further investigation regards the chemical and microstructural changes occurring between the different steps of the manufacturing cycle. While the present work shows a viable route for the manufacturing of patient-specific devices, the optimization of this route also for ensuring adequate fatigue properties requires further insights to the material's evolution during the manufacturing cycle. Future works will also assess the design of patient-specific devices employing the data gathered here as well as the criteria for parametric design starting from patient data. The present study was mainly aimed at biomedical device manufacturing. However, several results are beneficial for other applications that may require the use of micro struts. Lattice structures for lightweight design and vibration

management, strut-based actuators for microdevices will require similar properties, which were addressed in this work.

Acknowledgments

The authors gratefully acknowledge the technical support provided by Alberto Coda and Jannis Lemke from SAES Getters Spa. The Italian Ministry of Education, University and Research is acknowledged for the support provided through the Project “Department of Excellence LIS4.0 - Lightweight and Smart Structures for Industry 4.0”.

References

- [1] A. Koptug, L.-E. Rännar, M. Bäckström, M.S.S. Fager Franzén, D.P. Dérand, Additive Manufacturing Technology Applications Targeting Practical Surgery, *Int. J. Life Sci. Med. Res.* 3 (2013) 15–24. doi:10.5963/LSMR0301003.
- [2] D. Kong, X. Ni, C. Dong, X. Lei, L. Zhang, C. Man, J. Yao, X. Cheng, X. Li, Bio-functional and anti-corrosive 3D printing 316L stainless steel fabricated by selective laser melting, *Mater. Des.* 152 (2018) 88–101. doi:10.1016/j.matdes.2018.04.058.
- [3] F.S. Schwindling, M. Seubert, S. Rues, U. Koke, M. Schmitter, T. Stober, Two-Body Wear of CoCr Fabricated by Selective Laser Melting Compared with Different Dental Alloys, *Tribol. Lett.* 60 (2015) 1–8. doi:10.1007/s11249-015-0601-7.
- [4] S.L. Sing, J. An, W.Y. Yeong, F.E. Wiria, Laser and electron-beam powder-bed additive manufacturing of metallic implants: A review on processes, materials and designs, *J. Orthop. Res.* 34 (2016) 369–385. doi:10.1002/jor.23075.
- [5] R. Stamp, P. Fox, W. O’Neill, E. Jones, C. Sutcliffe, The development of a scanning strategy for the manufacture of porous biomaterials by selective laser melting, *J. Mater. Sci. Mater. Med.* 20 (2009) 1839–1848. doi:10.1007/s10856-009-3763-8.
- [6] A.A. Oliver, M. Sikora-Jasinska, A.G. Demir, R.J. Guillory, Recent advances and directions in the development of bioresorbable metallic cardiovascular stents: Insights from recent human and in vivo studies, *Acta Biomater.* 127 (2021) 1–23. doi:10.1016/j.actbio.2021.03.058.
- [7] A. Raval, A. Choubey, C. Engineer, D. Kothwala, Development and assessment of 316LVM cardiovascular stents, *Mater. Sci. Eng. A.* 386 (2004) 331–343. doi:10.1016/j.msea.2004.07.051.
- [8] D. Stoeckel, C. Bonsignore, S. Duda, M. Dunitz, A survey of stent designs., *Minim. Invasive Ther. Allied Technol.* 11 (2002) 137–47. doi:10.1080/136457002760273340.
- [9] A.G. Demir, B. Previtali, Additive manufacturing of cardiovascular CoCr stents by selective laser melting, *Mater. Des.* 119 (2017) 338–350. doi:10.1016/j.matdes.2017.01.091.
- [10] Y. Wessarges, R. Hagemann, M. Gieseke, C. Nölke, S. Kaierle, W. Schmidt, K.-P. Schmitz, H. Haferkamp, Additive manufacturing of vascular implants by selective laser melting, *Biomed. Tech.* 59 (2014) S404. doi:10.1515/bmt-2014-5005.
- [11] L. Wiesent, U. Schultheiß, P. Lulla, U. Noster, T. Schratzenstaller, C. Schmid, A. Nonn, A. Spear, Computational analysis of the effects of geometric irregularities and post-processing steps on the mechanical behavior of additively manufactured 316L stainless steel stents, *PLoS One.* 15 (2020) 1–30. doi:10.1371/journal.pone.0244463.
- [12] P. Wen, M. Voshage, L. Jauer, Y. Chen, Y. Qin, R. Poprawe, J.H. Schleifenbaum, Laser additive manufacturing of Zn metal parts for biodegradable applications: Processing, formation quality and mechanical properties, *Mater. Des.* 155 (2018) 36–45. doi:10.1016/J.MATDES.2018.05.057.
- [13] J. Hufenbach, J. Sander, F. Kochta, S. Pilz, A. Voss, U. Kühn, A. Gebert, Effect of Selective Laser Melting on Microstructure, Mechanical, and Corrosion Properties of Biodegradable FeMnCS for Implant Applications, *Adv. Eng. Mater.* 22 (2020) 1–8. doi:10.1002/adem.202000182.
- [14] V. Finazzi, A.G. Demir, C.A. Biffi, C. Chiastra, F. Migliavacca, L. Petrini, B. Previtali, Design Rules for Producing Cardiovascular Stents by Selective Laser Melting: Geometrical Constraints and Opportunities, *Procedia Struct. Integr.* 15 (2019) 16–23. doi:10.1016/j.prostr.2019.07.004.
- [15] S. Maffia, V. Finazzi, F. Berti, F. Migliavacca, L. Petrini, B. Previtali, A.G. Demir, Selective laser melting of NiTi stents with open-cell and variable diameter, *Smart Mater. Struct.* 30 (2021) 105010. doi:10.1088/1361-665X/ac1908.
- [16] P. Jamshidi, C. Panwisawas, E. Langi, S.C. Cox, J. Feng, L. Zhao, M.M. Attallah, Development,

- characterisation, and modelling of processability of nitinol stents using laser powder bed fusion, *J. Alloys Compd.* 909 (2022) 164681. doi:10.1016/j.jallcom.2022.164681.
- [17] T.E. Abioye, P.K. Farayibi, P. Kinneil, A.T. Clare, Functionally graded Ni-Ti microstructures synthesised in process by direct laser metal deposition, *Int. J. Adv. Manuf. Technol.* 79 (2015) 843–850. doi:10.1007/s00170-015-6878-8.
- [18] J. Van Humbeeck, Additive Manufacturing of Shape Memory Alloys, *Shape Mem. Superelasticity.* 4 (2018) 309–312. doi:10.1007/s40830-018-0174-z.
- [19] C.A. Biffi, A. Tuissi, A.G. Demir, Martensitic transformation, microstructure and functional behavior of thin-walled Nitinol produced by micro laser metal wire deposition, *J. Mater. Res. Technol.* 12 (2021) 2205–2215. doi:10.1016/j.jmrt.2021.03.108.
- [20] S. Dadbakhsh, B. Vrancken, J.P. Kruth, J. Luyten, J. Van Humbeeck, Texture and anisotropy in selective laser melting of NiTi alloy, *Mater. Sci. Eng. A.* 650 (2016) 225–232. doi:10.1016/j.msea.2015.10.032.
- [21] S. Saedi, N. Shayesteh Moghaddam, A. Amerinatanzi, M. Elahinia, H.E. Karaca, On the effects of selective laser melting process parameters on microstructure and thermomechanical response of Ni-rich NiTi, *Acta Mater.* 144 (2018) 552–560. doi:10.1016/j.actamat.2017.10.072.
- [22] L. Xue, K.C. Atli, C. Zhang, N. Hite, A. Srivastava, A.C. Leff, A.A. Wilson, D.J. Sharar, A. Elwany, R. Arroyave, I. Karaman, Laser Powder Bed Fusion of Defect-Free NiTi Shape Memory Alloy Parts with Superior Tensile Superelasticity, *Acta Mater.* 229 (2022) 117781. doi:10.1016/j.actamat.2022.117781.
- [23] M. Nematollahi, S.E. Saghaian, K. Safaei, P. Bayati, P. Bassani, C. Biffi, A. Tuissi, H. Karaca, M. Elahinia, Building orientation-structure-property in laser powder bed fusion of NiTi shape memory alloy, *J. Alloys Compd.* 873 (2021) 159791. doi:10.1016/j.jallcom.2021.159791.
- [24] A. Nespoli, P. Bettini, E. Villa, G. Sala, F. Passaretti, A.M. Grande, A Study on Damping Property of NiTi Elements Produced by Selective Laser-Beam Melting, *Adv. Eng. Mater.* 2001246 (2021) 1–9. doi:10.1002/adem.202001246.
- [25] C.A. Biffi, P. Bassani, J. Fiocchi, A. Tuissi, Microstructural and mechanical response of Niti lattice 3D structure produced by selective laser melting, *Metals (Basel).* 10 (2020) 1–9. doi:10.3390/met10060814.
- [26] A. Nespoli, A.M. Grande, N. Bennato, D. Rigamonti, P. Bettini, E. Villa, G. Sala, F. Passaretti, Towards an understanding of the functional properties of NiTi produced by powder bed fusion, *Prog. Addit. Manuf.* 6 (2021) 321–337. doi:10.1007/s40964-020-00155-1.
- [27] N. Shayesteh Moghaddam, S. Saedi, A. Amerinatanzi, A. Hinojos, A. Ramazani, J. Kundin, M.J. Mills, H. Karaca, M. Elahinia, Achieving superelasticity in additively manufactured NiTi in compression without post-process heat treatment, *Sci. Rep.* 9 (2019) 1–11. doi:10.1038/s41598-018-36641-4.
- [28] T. Bormann, R. Schumacher, B. Müller, M. Mertmann, M. De Wild, Tailoring selective laser melting process parameters for niti implants, *J. Mater. Eng. Perform.* 21 (2012) 2519–2524. doi:10.1007/s11665-012-0318-9.
- [29] S. Saedi, A.S. Turabi, M.T. Andani, C. Haberland, H. Karaca, M. Elahinia, The influence of heat treatment on the thermomechanical response of Ni-rich NiTi alloys manufactured by selective laser melting, *J. Alloys Compd.* 677 (2016) 204–210. doi:10.1016/j.jallcom.2016.03.161.
- [30] C.A. Biffi, J. Fiocchi, F. Valenza, P. Bassani, A. Tuissi, Selective Laser Melting of NiTi Shape Memory Alloy: Processability, Microstructure, and Superelasticity, *Shape Mem. Superelasticity.* 6 (2020) 342–353. doi:10.1007/s40830-020-00298-8.
- [31] K. Khanlari, Q. Shi, K. Li, K. Hu, P. Cao, X. Liu, Effects of printing volumetric energy densities and post-processing treatments on the microstructural properties, phase transformation temperatures and hardness of near-equiatomic NiTiInol parts fabricated by a laser powder bed fusion technique, *Intermetallics.* 131 (2021). doi:10.1016/j.intermet.2021.107088.
- [32] X. Wang, S. Kustov, J. Van Humbeeck, A short review on the microstructure, transformation behavior and functional properties of NiTi shape memory alloys fabricated by selective laser melting, *Materials (Basel).* 11 (2018). doi:10.3390/ma11091683.
- [33] J. Frenzel, E.P. George, A. Dlouhy, C. Somsen, M.F.X. Wagner, G. Eggeler, Influence of Ni on martensitic phase transformations in NiTi shape memory alloys, *Acta Mater.* 58 (2010) 3444–3458. doi:10.1016/j.actamat.2010.02.019.
- [34] O.F. Bertrand, R. Sipehia, R. Mongrain, J. Rodés, J.C. Tardif, L. Bilodeau, G. Côté, M.G. Bourassa,

- Biocompatibility aspects of new stent technology., *J. Am. Coll. Cardiol.* 32 (1998) 562–71.
<http://www.ncbi.nlm.nih.gov/pubmed/9741494>.
- [35] D. Carluccio, A.G. Demir, L. Caprio, B. Previtali, M.J. Bermingham, M.S. Dargusch, The influence of laser processing parameters on the densification and surface morphology of pure Fe and Fe-35Mn scaffolds produced by selective laser melting, *J. Manuf. Process.* 40 (2019) 113–121.
 doi:10.1016/j.jmapro.2019.03.018.
 - [36] F. Guaglione, L. Caprio, B. Previtali, A.G. Demir, Single point exposure LPBF for the production of biodegradable Zn-alloy lattice structures, *Addit. Manuf.* (2021) 102426.
 doi:10.1016/j.addma.2021.102426.
 - [37] E. Vasileska, A.G. Demir, B.M. Colosimo, B. Previtali, Layer-wise control of selective laser melting by means of inline melt pool area measurements, *J. Laser Appl.* 32 (2020) 022057.
 doi:10.2351/7.0000108.
 - [38] V. Finazzi, A.G. Demir, C.A. Biffi, F. Migliavacca, L. Petrini, B. Previtali, Design and functional testing of a novel balloon-expandable cardiovascular stent in CoCr alloy produced by selective laser melting, *J. Manuf. Process.* 55 (2020) 161–173. doi:10.1016/j.jmapro.2020.03.060.
 - [39] H. Liang, D. Xie, Y. Mao, J. Shi, C. Wang, L. Shen, Z. Tian, The size effect on forming quality of Ti-6Al-4V solid struts fabricated via laser powder bed fusion, *Metals (Basel)*. 9 (2019).
 doi:10.3390/met9040416.
 - [40] M. Gavazzoni, L. Boniotti, S. Foletti, Influence of specimen size on the mechanical properties of microlattices obtained by selective laser melting, *Proc. Inst. Mech. Eng. Part C J. Mech. Eng. Sci.* 0 (2019) 1–14. doi:10.1177/0954406219869741.
 - [41] E. Maleki, S. Bagherifard, M. Bandini, M. Guagliano, Surface post-treatments for metal additive manufacturing: Progress, challenges, and opportunities, *Addit. Manuf.* 37 (2021) 101619.
 - [42] H. Zhao, R. Stalmans, J. van Humbeeck, I. de Scheerder, Pickling of laser-cut NiTi slotted tube stents: Effect on surface morphology, dimension changes and mechanical behaviour, *J. Phys. IV*. 112 (2003) 1125–1128. doi:10.1051/jp4:20031080.
 - [43] A.G. Demir, B. Previtali, Comparative study of CW, nanosecond- and femtosecond-pulsed laser microcutting of AZ31 magnesium alloy stents, *Biointerphases*. 9 (2014) 029004.
 doi:10.1116/1.4866589.
 - [44] A.G. Demir, B. Previtali, C.A. Biffi, Fibre Laser Cutting and Chemical Etching of AZ31 for Manufacturing Biodegradable Stents, *Adv. Mater. Sci. Eng.* 2013 (2013) 1–11.
 doi:10.1155/2013/692635.
 - [45] E. Dordoni, L. Petrini, W. Wu, F. Migliavacca, G. Dubini, G. Pennati, Computational Modeling to Predict Fatigue Behavior of NiTi Stents: What Do We Need?, *J. Funct. Biomater.* 6 (2015) 299–317.
 doi:10.3390/jfb6020299.
 - [46] ASTM International, ASTM F2063-05 - Standard Specification For Wrought Nickel-Titanium Shape Memory Alloys For Medical Devices And Surgical Implants, n.d.
 - [47] V. Finazzi, A.G. Demir, C.A. Biffi, F. Migliavacca, L. Petrini, B. Previtali, Design and functional testing of a novel balloon-expandable cardiovascular stent in CoCr alloy produced by selective laser melting, *J. Manuf. Process.* 55 (2020) 161–173. doi:10.1016/j.jmapro.2020.03.060.
 - [48] S. Maffia, V. Finazzi, F. Berti, F. Migliavacca, L. Petrini, B. Previtali, A.G. Demir, Selective laser melting of NiTi stents with open-cell and variable diameter, *Smart Mater. Struct.* 30 (2021).
 doi:10.1088/1361-665X/ac1908.
 - [49] A.B. Spierings, G. Levy, Comparison of density of stainless steel 316L parts produced with selective laser melting using different powder grades, in: *Proc. Solid Free. Fabr. Symp.*, 2009: pp. 342–353.
 - [50] ISO - ISO 4287:1997 - Geometrical Product Specifications (GPS) — Surface texture: Profile method — Terms, definitions and surface texture parameters, (n.d.).
 - [51] ISO - ISO 4288:1996/Cor 1:1998 - Geometrical Product Specifications (GPS) — Surface texture: Profile method — Rules and procedures for the assessment of surface texture — Technical Corrigendum 1, (n.d.).
 - [52] M. Tang, P.C. Pistorius, J.L. Beuth, Prediction of lack-of-fusion porosity for powder bed fusion, *Addit. Manuf.* 14 (2017) 39–48. doi://doi.org/10.1016/j.addma.2016.12.001.
 - [53] V.D. Le, E. Pessard, F. Morel, F. Edy, Influence of porosity on the fatigue behaviour of additively fabricated TA6V alloys, *MATEC Web Conf.* 165 (2018) 1–9. doi:10.1051/mateconf/201816502008.
 - [54] M. Jaskari, J. Mäkikangas, A. Järvenpää, K. Mäntyjärvi, P. Karjalainen, Effect of high porosity on bending fatigue properties of 3D printed AISI 316L steel, *Procedia Manuf.* 36 (2019) 33–41.

doi:10.1016/j.promfg.2019.08.006.

- [55] S. Hatami, T. Ma, T. Vuoristo, J. Bertilsson, O. Lyckfeldt, Fatigue Strength of 316 L Stainless Steel Manufactured by Selective Laser Melting, *J. Mater. Eng. Perform.* 29 (2020) 3183–3194. doi:10.1007/s11665-020-04859-x.
- [56] G. Carlucci, L. Patriarca, A.G. Demir, J.N. Lemke, A. Coda, B. Previtali, R. Casati, Building Orientation and Heat Treatments Effect on the Pseudoelastic Properties of NiTi Produced by LPBF, *Shape Mem. Superelasticity.* (2022). doi:10.1007/s40830-022-00391-0.
- [57] ASTM International, F2004-17 Standard Test Method for Transformation Temperature of Nickel-Titanium Alloys by Thermal Analysis, (2017). doi:https://doi.org/10.1520/F2004-17.
- [58] ASTM International, F2516 Tension Testing of Nickel-Titanium Superelastic Materials, (2018) 1–8. doi:10.1520/F2516-18.2.
- [59] V. Finazzi, F. Berti, R.J. Guillory II, L. Petrini, B. Previtali, A.G. Demir, Patient-specific cardiovascular superelastic NiTi stents produced by laser powder bed fusion, *Procedia CIRP.* 110 (2022) 242–246. doi:10.1016/j.procir.2022.06.044.
- [60] Endologix, Alto™ Abdominal Stent Graft System – P120006/S031, FDA Recent. Approv. Devices. (2022). <https://www.fda.gov/medical-devices/recently-approved-devices/altotm-abdominal-stent-graft-system-p120006s031>.
- [61] ID Nest Medical, ID Venous System, (2022). <https://www.idnest-medical.com/en/id-venous-system/%0B> (accessed November 5, 2022).
- [62] T.W. Duerig, A.R. Pelton, K. Bhattacharya, The Measurement and Interpretation of Transformation Temperatures in Nitinol, *Shape Mem. Superelasticity.* 3 (2017) 485–498. doi:10.1007/s40830-017-0133-0.
- [63] F. Ahmed, U. Ali, D. Sarker, E. Marzbanrad, K. Choi, Y. Mahmoodkhani, E. Toyserkani, Study of powder recycling and its effect on printed parts during laser powder-bed fusion of 17-4 PH stainless steel, *J. Mater. Process. Technol.* 278 (2020) 116522. doi:10.1016/j.jmatprotec.2019.116522.
- [64] S. Cacace, V. Furlan, R. Sorci, Q. Semeraro, M. Boccadoro, Using recycled material to produce gas-atomized metal powders for additive manufacturing processes, *J. Clean. Prod.* 268 (2020) 122218. doi:10.1016/j.jclepro.2020.122218.
- [65] M.I. Khan, A. Pequegnat, Y.N. Zhou, Multiple memory shape memory alloys, *Adv. Eng. Mater.* 15 (2013) 386–393. doi:10.1002/adem.201200246.
- [66] A.R. Pelton, S.M. Russell, J. DiCello, The physical metallurgy of Nitinol for medical applications, *Jom.* 55 (2003) 33–37. doi:10.1007/s11837-003-0243-3.
- [67] M. Costas, D. Morin, M. de Lucio, M. Langseth, Testing and simulation of additively manufactured AlSi10Mg components under quasi-static loading, *Eur. J. Mech. A/Solids.* 81 (2020) 103966. doi:10.1016/j.euromechsol.2020.103966.
- [68] K. Karolewska, B. Ligaj, M. Wirwicki, G. Szala, Strength analysis of Ti6Al4V titanium alloy produced by the use of additive manufacturing method under static load conditions, *J. Mater. Res. Technol.* 9 (2020) 1365–1379. doi:10.1016/j.jmrt.2019.11.063.
- [69] K. Dietrich, J. Diller, S. Dubiez-Le Goff, D. Bauer, P. Forêt, G. Witt, The influence of oxygen on the chemical composition and mechanical properties of Ti-6Al-4V during laser powder bed fusion (LPBF), *Addit. Manuf.* 32 (2020). doi:10.1016/j.addma.2019.100980.
- [70] M. Simonelli, Y.Y. Tse, C. Tuck, Effect of the build orientation on the mechanical properties and fracture modes of SLM Ti-6Al-4V, *Mater. Sci. Eng. A.* 616 (2014) 1–11. doi:10.1016/j.msea.2014.07.086.
- [71] F. Berti, A. Spagnoli, L. Petrini, A numerical investigation on multiaxial fatigue assessment of Nitinol peripheral endovascular devices with emphasis on load non-proportionality effects, *Eng. Fract. Mech.* (2019) 106512. doi:10.1016/J.ENGFRACMECH.2019.106512.